10/13-93 JS (2)

PREPARED FOR THE U.S. DEPARTMENT OF ENERGY,
UNDER CONTRACT DE-AC02-76-CHO-3073

PPPL-2916
UC-420

PPPL-2916

EXCITATION OF HIGH FREQUENCY PRESSURE DRIVEN MODES BY NON-AXISYMMETRIC EQUILIBRIUM AT HIGH β_{pol} IN PBX-M

BY

S. SESNIC, A. HOLLAND, R. KAITA, ET AL.

JUNE, 1993

PRINCETON
PLASMA PHYSICS
LABORATORY

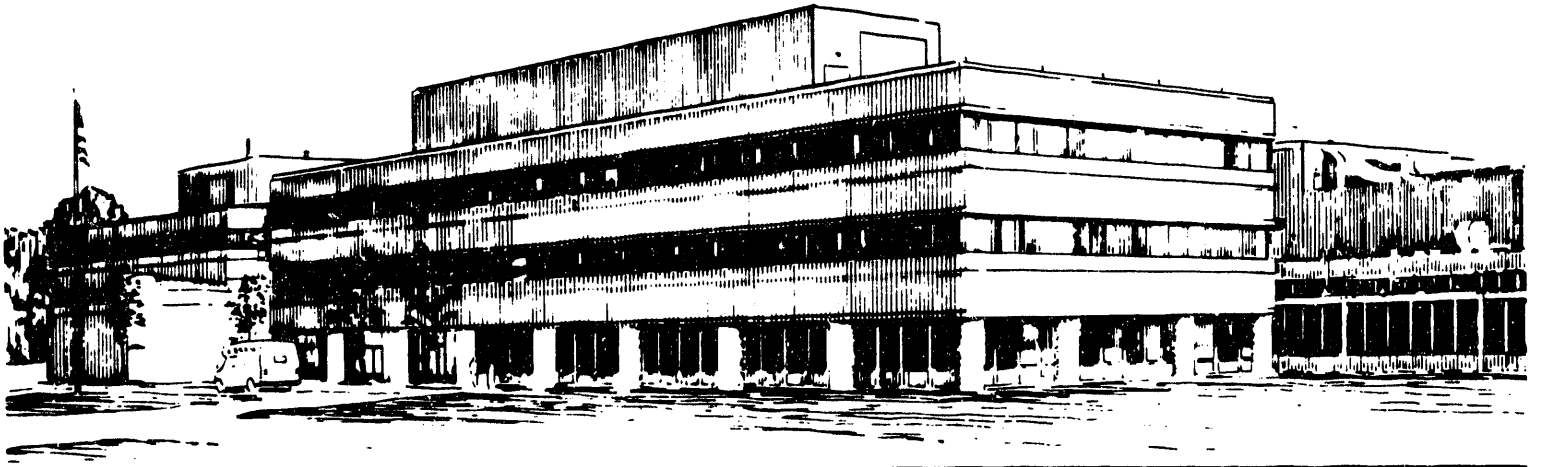

PRINCETON UNIVERSITY, PRINCETON, NEW JERSEY

DISTRIBUTION OF THIS DOCUMENT IS UNLIMITED

NOTICE

This report was prepared as an account of work sponsored by an agency of the United States Government. Neither the United States Government nor any agency thereof, nor any of their employees, makes any warranty, express or implied, or assumes any legal liability or responsibility for the accuracy, completeness, or usefulness of any information, apparatus, product, or process disclosed, or represents that its use would not infringe privately owned rights. Reference herein to any specific commercial produce, process, or service by trade name, trademark, manufacturer, or otherwise, does not necessarily constitute or imply its endorsement, recommendation, or favoring by the United States Government or any agency thereof. The views and opinions of authors expressed herein do not necessarily state or reflect those of the United States Government or any agency thereof.

NOTICE

This report has been reproduced from the best available copy.
Available in paper copy and microfiche.

Number of pages in this report: 46

DOE and DOE contractors can obtain copies of this report from:

Office of Scientific and Technical Information
P.O. Box 62
Oak Ridge, TN 37831;
(615) 576-8401.

This report is publicly available from the:

National Technical Information Service
Department of Commerce
5285 Port Royal Road
Springfield, Virginia 22161
(703) 487-4650

EXCITATION OF HIGH FREQUENCY PRESSURE DRIVEN MODES BY NON-AXISYMMETRIC EQUILIBRIUM AT HIGH β_{pol} IN PBX-M

S. SESNIC, A. HOLLAND[a], R. KAITA, S. KAYE, M. OKABAYASHI, H. TAKAHASHI, N. ASAKURA[b], R.E. BELL, S. BERNABEI, M.S. CHANCE, P.-A. DUPERREX[c], R.J. FONCK[d], G.M. GAMMEL[e], G.J. GREENE[f], R.E. HATCHER, S.C. JARDIN, T.-W. JIANG[g], C.E. KESSEL, H.W. KUGEL, B. LEBLANC, F.M. LEVINTON[h], J. MANICKAM, M. ONO, S.F. PAUL, E.T. POWELL[i], Y. QIN[j], D.W. ROBERTS[i], and N.R. SAUTHOFF

Princeton Plasma Physics Laboratory, Princeton University
P. O. Box 451
Princeton, New Jersey 08543,
USA

ABSTRACT

High-frequency pressure-driven modes have been observed in high-poloidal-β discharges in the Princeton Beta Experiment-Modification (PBX-M). These modes are excited in a non-axisymmetric equilibrium characterized by a large, low frequency $m_l=1/n_l=1$ island, and they are capable of expelling fast ions. The modes reside on or very close to the q=1 surface, and have mode numbers with either $m_h=n_h$ or (less probably) $m_h/n_h=m_h/(m_h-1)$, with m_h varying between 3 and 10. Occasionally, these modes are simultaneously localized in the vicinity of the $m_l=2/n_l=1$ island. The high frequency modes near the q=1 surface also exhibit a ballooning character, being significantly stronger on the large major radius side of the plasma. When a large $m_l=1/n_l=1$ island is present the mode is poloidally localized in the immediate vicinity of the x-point of the island. The modes, which occur exclusively in high-β discharges, appear to be driven by the plasma pressure or pressure gradient. They can thus be a manifestation of either a toroidicity-induced shear Alfvén eigenmode (TAE) at $q=(2m_h+1)/2n_h$, a kinetic ballooning mode (KBM), or some other type of pressure-driven mode. Theory predicts that the TAE mode is a gap mode, but the high frequency modes in PBX-M are found exclusively on or in the immediate neighborhood of magnetic surfaces with low rational numbers (q=1, 2, ..).

MASTER

1. INTRODUCTION

The central purpose of the Princeton Beta Experiment-Modification (PBX-M) is to achieve and explore the second regime of stability to ideal ballooning modes. To effect this goal, the PBX-M program has focussed on plasmas in two operating domains. The first was characterized by high plasma current relative to minor radius and magnetic field ($I/aB \approx$ 2.1 MA/m-T). In this scenario, a rapid current ramp (up to 2.4 MA/sec) broadened the current profile by adding edge current. These plasmas had values of the volume-averaged toroidal beta, $<\beta_t>$, up to 6.8%, and a maximum normalized beta, $<\beta_n> = <\beta_t>/(I/aB)$, of 3.5%-m-T/MA.[1,2] The objective of the high-$<\beta_n>$ operating regime was to approach the threshold of second stability with plasmas at high values of poloidal beta ($\beta_{pol}=8W_{tot}/(3\mu_o R_o I_p^2) \approx 2.4$). At moderate I/aB ($\approx$ 0.9 MA/m-T), a β_n of 4.5 was achieved.

Strong high frequency MHD phenomena that appear to be related to plasma pressure have been observed in several tokamaks. Deuterium neutral beams with energies up to 110 keV were injected into plasmas with low magnetic fields (1T) in TFTR.[3,4] The beam injection velocities (v_f) were comparable to the Alfvén velocity (v_A), so that toroidicity-induced shear Alfvén eigenmodes (TAE) were excited. There was a clear correlation between the high-frequency (h. f.) bursts in the Mirnov coil signal and decreases in the neutron emission rate. In DIII-D experiments with low magnetic fields (0.6 - 1.4T), magnetic oscillations in the TAE range (50-200 kHz) were also detected during neutral beam injection.[5,6] Beam power losses of over 50% were reported at the largest TAE amplitudes. A sharp onset threshold at $v_f/v_A = 1$ was not observed, which is consistent with the theoretical prediction that sideband coupling permits the mode to be driven by fast ions as slow as $v_f \approx v_A/3$. This suggests that the instabilities first observed with tangential neutral beam injection in high-β PBX plasmas were indeed TAE; although the fast ion velocities were substantially below v_A, h. f. bursts were detected with the Mirnov coils, and they were clearly correlated with significant changes in the neutron emissivity.[7] A somewhat different ballooning mode of much lower frequency (36 kHz), with an m/n=7/6 "wave packet" character that was stationary in the moving plasma frame, was observed in TFTR.[8].

Modes very similar to those seen in TFTR, D-III-D, and PBX have been found during the 1988/1989 experimental period on PBX-M.[1,2,9] The experimental conditions under which these modes were observed included high values of β_{pol} and β_n, which were around 2 and 4 respectively. These values were achieved with neutral beam injection, P_b, of 5

MW, plasma current, I_p, of 320 to 350 kA, toroidal magnetic field, B_t, of 1.3 T, electron temperature of 2 keV, ion temperature of 4 keV, elongation of 1.9, indentation of 15%-18%, and triangularity of 0.3. The neutral beam power at an injection energy of 40 keV was approximately equally divided into near-parallel (tangency radius: R_{tan}=130 cm) and near-perpendicular (R_{tan}=35 cm) directions.

Typical equilibrium magnetic surfaces for the high-β_{pol} case are shown in Fig. 1. MHD mode activity in these H-mode discharges varied as the discharge progressed. Representative plasma parameters for a typical high-β_{pol} discharge are shown in Fig. 2, where an H-mode sets in at 360 ms. During the last phase of the β-increase period, sawteeth and very weak low-n modes are observed. The β-saturation period is characterized by sawteeth, weaker n=1 to 3 modes, grassy ELM-like events, and isolated weak ELM's. Grassy ELM-like events are edge phenomena propagating in a finite time toward the center of the discharge. They induce energy losses between 1 to 2% and have repetition rates of 0.5 to 2 kHz, and they seem to be mainly responsible for the β-saturation. In Fig. 2, there are two such periods where the β saturates: one from 460 to 490 ms and the other from 510 to 535 ms. The β-collapse is normally initiated by a giant ELM (at 535ms in Fig. 2), followed by very strong low-n activity (primarily n = 1 but occasionally having n values up to 4), interspersed with additional giant ELM's. Giant ELM's in PBX-M are ELM's of very short duration ($\approx$ 500μs) and are associated with very large plasma energy losses (between 10 to 30%). It is during these three periods that the high frequency (h.f.) mode activity was observed.

The diagnostics used to obtain the principal measurements in the present report were the soft x-ray diode array, motional Stark effect (MSE) polarimetry, and the neutron fluctuation diagnostic. The sightlines of the 32 soft X-ray diodes are shown in Fig. 1. The array provides coverage of the poloidal cross section of the plasma with 2 cm spatial resolution. The MSE technique was pioneered on PBX-M as a means of obtaining q profiles in high temperature tokamak plasmas.[10] The motion of a neutral hydrogen beam across the confining magnetic field introduces a Stark splitting in the H_α emission. The photons are polarized in the direction of the magnetic field, and local values of q are determined from the intersection of the polarimeter sightline and the trajectory of the horizontally-scanning neutral probe beam.[11] The neutron fluctuation diagnostic consists of two counters, a plastic scintillator (NE102) for fast time resolution and a thin ZnS scintillator (NE422) with less sensitivity to hard X-rays.[12] Correlations with other diagnostics were made using data primarily from the NE422 detector.

The present work focuses on three areas: the detailed internal structure of the mode

(amplitude and phase profiles); clear establishment of a strong ballooning character for this mode; and, finally, recognition for the first time of the importance of a strongly non-axisymmetric equilibrium for the excitation and the strength of this mode.

The experimental results are described in the second section: the spectral structure of these modes; their localization and their spatial structure in minor radius relative to their corresponding q-values; identification of m- and n-numbers; central fast ion losses and central electron thermal energy losses; and in summary, a physical picture for these modes. In the third section the data are compared with several fast ion theories, suggesting TAE or KBM as the two possible explanations for these modes.

2. EXPERIMENTAL OBSERVATIONS

2.1. Spectral Structure of the Modes

The β-saturation and β-collapse periods in the high-β_{pol}, high-Troyon parameter discharges in PBX-M are characterized by strong MHD activity. Very often we observe giant ELMs with a repetition rate on the order of 10 ms, and a strong saturated n=1 mode with a frequency of 7 kHz. In addition, we sometimes observe high frequency bursting at 100 kHz and above. The high frequency mode appears as a sequence of bursts because it is modulated by the n_l=1, low frequency (l.f.) mode. This modulation is a case of a nonlinear interaction of two modes, a low-frequency/low-n and a high-frequency/high-n mode, localized very near each other.

A typical case of such a nonlinear interaction is shown in Fig. 3, where soft x-ray diode signals for the central part of the plasma are depicted. The h. f. mode is observed only during the crest of the l. f. mode, and it rotates with the crest of that mode in the poloidal and/or toroidal direction. The top and the bottom signals are coming from the plasma shell located roughly in the vicinity of the q=1 surface. Two signals from the same diode are overlayed on each other: in one case the signal is digitally filtered with a high pass filter of 0.5 kHz and in the other case with a high pass filter of 90 kHz. The h. f. mode is observed primarily in the central part of the plasma, so that the nonlinear interaction of the h. f. mode occurs mainly with the m_l=1 component of the global n_l=1 eigenmode. The l. f. n_l=1 mode has a strong m_l=1 central component.

If the maximum soft x-ray radiation occurs around the x-point of an m_l=1 island, and this perturbation has an island structure, Fig. 3 suggests that the h. f. mode is localized

near the x-point of the low frequency $m_l=1/n_l=1$ mode. The h. f. perturbation (or h.f. burst), carried on top of the crest of the l. f. perturbation, is observed in a particular diode only during the passage of the l. f. crest in front of that diode. The burst itself thus shows a "light-house" effect, i.e., a beacon rotating poloidally or toroidally which follows a helical line in the torus defined by the crest of the $m_l=1/n_l=1$ mode. Other features in Fig. 3 are described in sections below.

The Fourier power spectrum analysis of these signals for the central part of the plasma is shown in Fig. 4. The l. f. part of the spectra is omitted from the figure because of the very large amplitude of the low frequency mode. We note that in the central part of the plasma there are many peaks between 70 and 180 kHz. In some cases over fifteen simultaneous h.f. peaks are observed. They are regularly spaced, and their separation on average is 7.3 kHz. This separation is equal to the frequency of the l. f. mode. The h. f. mode disappears outside z=23 cm, which is equivalent to a midplane minor radius, r_{mid}, of 14 cm. The integration time needed to obtain these spectra is 2 ms. Longer time windows cause the individual peaks to broaden and even to overlap into a single broad peak, due to the changing frequency of the h.f. mode with time.

The spectral structure of Fig. 4 with many h.f. peaks is to a large degree explained by the very non-sinusoidal modulation (envelope) of the h.f. mode with the l.f. mode (Fig. 3). The fact that the l.f. envelope of the h.f. mode is so strongly non-sinusoidal will create many strong sidebands around the frequency, ω_h, of the h.f. mode. The amplitude of the sideband peaks (Fig. 4) is proportional to the degree of the distortion of the envelope of the h.f. mode in the time domain (Fig. 3). These sidebands are defined by $\omega_h \pm k\omega_l / m_h \pm km_l / n_h \pm kn_l$, where ω_l is the l.f. mode frequency, m_h, n_h ,$m_l=1$, and $n_l=1$ are poloidal and toroidal mode number of the h.f. and l.f. perturbation respectively, and k is an integer, k = 0, 1, 2, 3, ... Because the l.f. envelope of the h.f. mode can be assumed to be an even function, the power spectrum of Fig. 3, shown in Fig.4, is, therefore, described by a Fourier series $S(t, \omega_h, \omega_l) = \Sigma_k a_n \cos(\omega_h \pm k\omega_l)$. Σ_k denotes the summation over all k's. The coefficient a_n converges rather slowly, because of the strong distortion of the envelope. This is reflected in the many strong peaks of Fig 4.

2.2. Spatial Localization of the Mode

2.2.1. H.F. Mode Localized Near q = 1

In order to localize the mode and give some indication of the m- and n-number of the

mode, we have obtained the spatial profiles of the auto power spectra and the cross phase for a given peak in the high frequency spectrum. Such an analysis of the peaks at 103, 110, 118, and 125 kHz in Fig. 4 is shown in Figs. 5 and 7. From Fig. 5 one can conclude that the modes are localized inside z=20 cm or r_{mid} = 12 cm. r_{mid} is the midplane minor radius of the magnetic surface on which the diode sightline (identified by the vertical position z) is tangent. Their amplitudes fall precipitously outside z=20 cm (traces H2, H3, H4 and H5) and disappear into the photon noise (trace Ph). Because the steep outside wings (z>20 cm) of the h.f. mode profile follow closely those of the l.f. mode profile (trace L1), and the l.f. mode is an $m_l=1/n_l=1$ mode, one can conclude that the h.f. mode is localized either on or very near the q=1 surface. The jaggedness of the central part of the profile is real, and could be caused by the diode line-of-sight passing twice through the perturbed shell, i.e., once each on its large and small major radius side. The oscillations thus reflect the in-phase or out-of-phase superposition of these two contributions. Another possibility is that this profile jaggedness is caused by a fixed poloidal phase relationship between the l.f. and h.f. modes, which result in a standing wave pattern in the h.f. mode amplitude. In either case, from the number of peaks and valleys, the m-number must be higher than 3.

The power spectrum profile for most of these spectral peaks is broad and, despite the jaggedness, fairly flat inside z=20 cm. We thus conclude that the mode is localized in a narrow shell just inside z=20 cm and outside z=15 cm, i.e., the mode probably does not extend much toward the center.

2.2.2. A More Global H.F. Mode

A somewhat different case of h.f. modes is shown in Fig. 6. Here the normalized soft x-ray spectral profiles, S_f/S_o, of three of these modes (96, 103, and 110 kHz) and the low frequency n=1 mode are shown.

Before discussing the h.f. mode further, we describe the l.f. mode and locate the positions of the q=1, 2 surfaces from the power profile of the l.f. mode. The spectral power in the l.f. mode is more than an order of magnitude larger than for the h.f. modes. In addition, the low frequency mode has at least three maxima, an indication of a saturated global mode with strong m_l=1, 2, 3, ... components (islands). Motional Stark Effect (MSE) measurements of the q profile have been made on similar discharges, and they show that the locations of the q=1, q=2, and q=3 surfaces are located around z=20, 40, and 47 cm, agreeing well with the locations of the m_l=1, 2, 3 components of the n_l=1 mode shown in Fig 6. (The comments regarding l.f. mode are also valid for the case described in

Section 2.2.1.).

Unlike Fig.5, where the h.f. mode was sharply localized, this h.f. mode shows more of the character of a global mode with amplitude peaks: one just outside z=15 cm and the other near and outside z=25 cm. This puts the location of the internal peaks of the h.f. modes very near or just outside the the q=1 surface.

The external peaks of the h.f. mode follow closely the shape of the $m_l=2/n_l=1$ component of the l.f. mode, suggesting that this component of the h.f. mode is localized very near the q=2 surface. The amplitude of the external peak is smaller than the internal peak amplitude by more than factor of 5, and the soft x-ray array resolution around the q=2 surface is rather poor. It is thus impossible to establish either the m- or n-number of this mode or the exact location of the mode relative to the q=2 surface. For the same reasons, it is not possible to say anything definite about the ballooning character of the external mode.

2.3. m- and n-Number of the Mode

The spatial profile of the phase of the successive frequency peaks in Fig. 5 (96, 103, 110, 118, and 125 kHz) are depicted in Fig. 7a. The phase changes monotonically across the center between z=20 and -20 cm. The total phase change, $\Delta\phi_h$, across the plasma between z≈+20 and -20 cm, which are the radial positions close to the magnetic surface where the perturbation resides, increases with each successive spectral peak. The phase change between two successive peaks, $\Delta\phi_m$, corresponds to a change in m_h-number of $\Delta m_h \approx \Delta\phi_m/\Delta\phi_g \approx 1$. $\Delta\phi_g=140^o$ is the corresponding poloidal geometry angle subtended by the two extreme diodes of Fig. 3. The m_h-mode number difference ($\Delta m_h \approx 1$) is to be expected if these reside on the m/n rational surfaces, with m_h and n_h increasing by 1 when moving inward toward the q=1 surface. As the spectral peaks become weaker, the phase difference $\Delta\phi_m$ becomes smaller (H4 and H5 in Fig. 7a). This smaller $\Delta\phi_m$ might be a consequence either of noise (weaker peaks) and/or the fact that these other peaks were more an artifact of the "light-house" effect. The photon noise contribution to these peaks becomes also substantial causing a "flattening" of the phase profile. Note also that the phase profiles for z>0 are more "noisy," and that the phase difference there is more difficult to establish. This is a consequence of the unexplained increase in noise in the diode signals for z>0.

The large phase change across the plasma for a given spectral peak is an indication that the m_h-number of the high frequency mode must be rather high. By simple comparison of

the phase profiles of the h.f. modes and l.f. harmonics in Fig. 7a and 7b, we can conclude that the 103 kHz mode should have an m_h-number of at least 3 but not larger than 5, the 110 kHz mode should be between 4 and 6, and so forth. We assume here that the h.f. mode with the same m_h-number as the l.f. harmonic has a similar phase profile. Note that as the l.f. harmonic numbers increase, and the amplitude of the l.f. harmonic becomes too weak and approaches the photon noise, the phase profile stops changing (curves L4 and L5 in Fig. 7b).

The m_h-number can be also found directly from the Fig. 3 (or Fig. 10) by noting that the total phase change across all the diodes from z=15.9 to -15.9 cm is approximately, $\Delta\phi_h=720°$. Since the geometrical angle between the two extreme diodes is $\Delta\phi_g=140°$, one gets $m_h=\Delta\phi_h/\Delta\phi_g=5.1$ for the m_h-number.

Because the h.f. modes are located either on or very near the q=1 surface, the toroidal n_h-number is either equal or very close to the m_h-number. If we assume that for the 110 kHz peak the m_h-number is 5, then the n_h-number is either $n_h=m_h=5$ or $n_h=m_h-1=4$. As already mentioned, the high m_h-number is impossible to analyze with the poloidal set of magnetic probes. The magnetic probe measurement of the toroidal mode number was not available for this experiment.

2.4. Fast Ion and Thermal Electron Losses

The h.f. bursts are accompanied by a weak drop in the neutron rate. Beam target and beam-beam reactions dominate in PBX-M plasmas, so this drop in neutron rate indicates a loss of fast ions from the center of the discharge. The correlation between the gradual decrease in neutron rate and h.f. bursts is seen in Fig. 8 between 550 to 552 ms, 554 to 556 ms, and 572 to 574 ms. The large drop in the neutron rate at 565 ms is caused by one neutral beam being switched off. For a typical h.f. burst of 2 to 3 ms duration, this loss in neutron rate could be as much as 10%. In some cases, we observe an increased activity of these h.f. bursts a few ms preceding a giant ELM. In Fig. 8, this is observed for the giant ELM's at 557 and 565 ms. These neutron rate losses are largest for the case of a strong, bursting h.f. mode, associated with a strong non-axisymmetric configuration caused by a large $m_l=1/n_l=1$ island. In the case of a weak non-axisymmetric (small $m_l=1/n_l=1$ island) and axisymmetric configuration (no $m_l=1/n_l=1$ island), it was difficult to correlate these modes with any neutron rate drop. The reason might be that the peak amplitude of a h.f. bursting mode in a strongly non-axisymmetric equilibrium is an order of magnitude greater than the amplitude of the continuous h.f. mode in an axisymmetric equilibrium, and is also

greater than the amplitude of the h.f. mode in a weakly non-axisymmetric equilibrium.

These h.f. bursts are accompanied by a drop in the central soft x-ray signals, not unlike the one accompanying a sawtooth crash. This indicates that the electron thermal energy is being lost from the center during the h.f. burst. As shown in Fig. 9, the loss in soft x-ray intensity, localized in the vicinity of the q=1 surface, can be as high as 10%. This drop in electron thermal energy looks very much like a sawtooth with an inversion radius of z = 22 cm. It is not a sawtooth, however, as the $m_l=1/n_l=1$ large island is not affected by this drop. In addition, a sawtooth crash has the largest drop in the center, indicating electron thermal loss everywhere inside the q=1 surface. In an h.f. electron thermal energy crash, however, the electron thermal energy is preferentially lost around z = 20 cm (Fig. 9), i.e., the loss is very localized. This is the position of either the $q_{TAE}=(2m_h+1)/2n_h$, $q=m_h/n_h=1$, or $q=m_h/(m_h-1)$ shells where these h.f. modes are situated. The crash in electron thermal energy is also not sudden, but is a slower process spread over the h.f burst duration. Finally, in a sawtooth, the time evolution of the neutron rate follows the drop in the electron thermal energy crash, and is of very short duration. In the h.f. burst, this loss in the neutron rate is spread over the duration of the h.f. burst.

The significance of the electron thermal energy loss is not fully clear. On one hand the loss of fast ions due to the h.f. mode burst could reduce the central heating of electrons by ions and, therefore, produce the local loss in electron energy on a local electron transport time scale. On the other hand, this could also represent a direct loss of electron (and ion) thermal energy due to the h.f. burst. The relative increase in the electron thermal energy outside the inversion radius is also very large (see Fig. 9), greater than expected from a sawtooth. The reason for this might be that the fast ions, expelled by the h.f. burst from the center of the discharge, are heating the electrons in the region between z=25 and 50 cm. If this sawtooth-like crash represents the fast ion loss, the data in Fig. 9 might even shed some light on the radial position of the fast ions expelled from the center by the h.f. mode (r_{mid} = 15.5 to 26.5 cm), and the amount of the energy loss due to the expelled fast ions.

3. PHENOMENOLOGICAL PICTURE OF L.F. AND H.F. MODES

3.1. Case of Strongly Non-Axisymmetric Configuration

An essential condition for exciting the h.f. bursting mode is a strong non-axisymmetric equilibrium in the form of a large $m_l=1/n_l=1$ island. This h.f. bursting perturbation is

excited either at or just outside the x-point (maximum of the mode) of the $m_l=1/n_l=1$ perturbation, i.e., it resides on a rational magnetic surface on or just outside the q=1 surface.

Table I lists three most probable sets of m/n or q values. This table is based on combining the best independent m-number estimates from the amplitude profile (number of peaks) and the slope of the phase profile. The n-number is determined from the m-number ($n_h=m_h$ or $n_h=m_h-1$), knowing that the mode is on or close to the q=1 surface. The first set corresponds to the assumption that the h.f. mode is a toroidicity induced Alfvén eigenmode (TAE mode), with its location given by $q_{TAE}=(2m_h+1)/2n_h$. Two other sets of m_h/n_h numbers reflect the uncertainty in exact localization of the h.f. mode. The S model (Single shell) is based on the assumption that the mode is localized exactly on the $q=m_h/n_h=1$ surface and the M model (Multiple shells) on the assumption that the h.f. modes are localized just outside the q=1 surface, i.e., on the $q=m_h/(m_h-1)$ surfaces.

a) TAE mode

The location of the h.f. mode is consistent with a TAE mode position of $q_{TAE}=(2m_h+1)/2n_h$. With $m_h=5/n_h=5$, q_{TAE} becomes equal to 11/10, which is so close to q=1 that it is hard to discriminate between the two locations. On the other hand, the h.f. modes in PBX-M are always observed on or in the immediate vicinity of the rational surfaces of low rational number (q=1, 2 ...) and never in between them. This suggests that the rational surfaces of low rational numbers may play a decisive role in the excitation of the h.f. modes.

b) Single Shell Model with $q=m_h/n_h=1$

This model assumes that the h.f. mode is located on a rational surface of low rational number. The mode is located on the q=1 surface, and since the average frequency of the h.f. mode is about 110 kHz we see from Table I that the dominant mode has approximately $m_h=5/n_h=5$. This model explains the many spectral peaks of Fig. 4 most directly as a Fourier expansion of a poloidally (and toroidally) distorted $m_h=5/n_h=5$ mode (the error in m_h and n_h being ± 1). The distortion is caused by a strong decay of the mode away from the x-point of the $m_l=1/n_l=1$ island, and its strong ballooning character. With this picture the 110 kHz peak represents the dominant $m_h=5/n_h=5$ mode, but the other peaks in the spectrum also reflect real component modes with m_h and n_h larger or smaller than 5, depending on the frequency of the peak. These modes, together with the dominant mode, add up to the observed, strongly-distorted perturbation.

The drawback of this model is that it does not explain the apparent narrowing of the h.f. mode profiles with each successive peak (see below).

b) Multiple Shells Model with $q=m_h/(m_h-1)$

This model is less likely, but it does explain the fact that the mode amplitude profile moves slightly inward with each successive peak in spectrum (see Figs. 5, 6, and 11). This small successive inward movement of the profile could be interpreted as each spectral peak representing a mode on its own rational surface $q=m_h/m_h-1$, where with each successive peak the number m_h (and $n_h=m_h-1$) is increased by 1, thereby making q value of the corresponding m_h and n_h numbers smaller and approaching 1.

A weakness of this model is that it is difficult to see how a set of these modes, on successive rational surfaces near q=1, can add up to the simple but distorted h.f. mode observed. Another complication is that each one of these modes, since they are independent modes, should be distorted by itself through the presence of the l.f. $m_l=1/n_l=1$ island. This distortion should generate a series of new sideband modes, with frequencies and m_h/n_h numbers given by the expression $f_h \pm k f_l$ / $m_h \pm k$ / $n_h \pm k$. This means that each spectral peak, representing one mode on one rational surface, is potentially contaminated by the sideband components of the other modes on other rational surfaces.

From all this, it is clear that the excitation and propagation of these high frequency modes is tightly coupled to their co-existence with the $m_l=1/n_l=1$ and possibly $m_l=2/n_l=1$ modes. These modes were mostly observed in conjunction with a strong $m_l=1$ mode. The condition for excitation of these bursting modes is a strongly non-axisymmetric equilibrium, created by a strong $m_l=1/n_l=1$ island (and occasionally, an $m_l=2/n_l=1$ island). From the amplitude and position of the $m_l=1/n_l=1$ mode and the soft x-ray intensity profile, a simple simulation model will give us the position and the size of the island. In the case described in Figs. 3 to 6, where the normalized maximum modulation, S_f/S_o, was 20%, the very strong h.f. bursting is excited by an m=1/n=1 island. It has the midplane position r_{mid11} = 14 cm and a midplane island width of w_{mid11} = 3.2 cm, values obtained from the island simulation. The strong influence of the non-axisymmetric equilibrium, caused by a large $m_l=1/n_l=1$ island, on the excitation of the h.f. mode has been observed exclusively during the β-collapse period.

All of these modes, whether described by the TAE, S, or M model, have the same frequency f_h in the stationary plasma frame. The measured frequency f_m is Doppler-shifted, and the Doppler shift is a function of the n_h-number of the mode and the toroidal velocity of the plasma at the position of the mode. Since the toroidal velocity can be established from the frequency of the $m_l=1/n_l=1$ mode, f_l, as $v_t = R f_l$, the h.f. frequency in the plasma frame is given by $f_h = f_m - n f_l$. For the above case of the strongly bursting mode, and with f_l = 7.3 kHz, this gives us f_h = 73 kHz; the mode is propagating in the

stationary plasma frame, in the fast ion direction (neutral beam injection) with the velocity of 7.6×10^7 cm/s. This velocity is very close to one-third of the Alfvén velocity for this plasma ($v_A = 2.4 \times 10^8$ cm/s).

3.1.1. Ballooning Character of L.F. and H.F. Modes

From the directions of plasma current, toroidal field, and the toroidal rotation of plasma, given by the direction of the neutral beam injection, one can surmise the poloidal and toroidal rotation of the low frequency $m_l=1/n_l=1$ mode. The poloidal direction of the $m_l=1/n_l=1$ mode rotation is top-to-bottom on the large major radius side and bottom-to-top on the small major radius side of the torus (see Fig. 3). In addition, for the top half of the discharge ($z>0$), the half-wavelength before the peak (x-point) is slower than the half-wavelength following the peak by almost 50%. The opposite is true for the bottom half of the discharge ($z<0$): the half-wavelength before the peak is faster than the half wavelength following the peak. This uneven poloidal rotation is mainly due to the $m_l=1/n_l=1$ mode ballooning, although the strong non-sinusoidal distortion of the signal due to the large size of the $m_l=1/n_l=1$ island will contribute to this effect.

This ballooning can be observed in Fig. 3. Normally, the central channels would show a double frequency with two peaks of equal amplitude for an $m_l=1$ mode. Each of these peaks would have up-down *apparent* phase velocities of the opposite sign, which just reflects the fact that the x-point on the large major radius side is rotating from top to bottom, and in the opposite direction on the small major radius side. Here we observe only one strong peak, and it moves up-down in the positive direction (broken line t/b in Fig. 3). The other peak, moving in the opposite direction, is smaller by a factor of at least 5 (line b/t). The strong peak thus represents the x-point on the large major radius side, and the weak peak represents the same x-point during the time it rotates on the small major radius side. This is a clear indication of the ballooning characteristic of the $m_l=1/n_l=1$ mode.

The displacement vector of the $m_l=1/n_l=1$ mode, $\xi_{11}=S\sim_{11}/\mathrm{grad}S$ (where $S\sim_{11}$ is the auto power spectrum or the mode amplitude, and S is the total (DC) soft x-ray intensity), is expected to be reduced at the large major radius side, because of the slightly larger gradS at the large major radius side (the profile asymmetry being a Shafranov shift and β-effect). However, the net effect is that the displacement vector is still much larger at the large major radius side than at the small major radius side, since $S\sim_{11}$ is more than five times larger at the large major radius side.

In addition, the maximum of the l.f. envelope of the h.f. mode burst is strongly shifted

toward the faster (steeper) half wavelength of the l.f. mode, i.e., toward the large major radius side: for $z<0$ it is preceding and for $z>0$ it is following the x-point. This is a clear indication that the h.f. mode is ballooning even more strongly than the l.f. mode. As a result of the stronger ballooning of the h.f. mode, the maximum of the h.f. burst (the envelope) needs less time (40 μs; see "h.f. max" line in Fig. 3) to pass from the top to the bottom diode than the $m_l=1/n_l=1$ maximum (55 μs; "l.f. max" line). Another strong indication of the ballooning character of the high frequency mode is, just like in the case of the $m_l=1/n_l=1$ mode, the preferred direction of the poloidal rotation: the h.f. amplitude peak is moving from the top diode to the bottom diode, consistent with the h.f. perturbation localization on the large side of the major radius.

Because the amplitude profile of the h.f. mode is radially modulated with peaks and valleys, this also might indicate that the amplitude of the h.f. mode on the small major radius side is not zero but finite. However, a rather shallow depth of the modulation is an indication that the h.f. mode amplitude at the small radius side is much smaller than at the large major radius side. This also supports the ballooning character of the h.f. mode.

Another reason for the jaggedness of the profile is that two modes (h.f. and l.f.) have a fixed poloidal relationship due to the fact that the h.f. mode frequency seems to exactly coincide with the frequency of one l.f. harmonic ($f_h=15f_l$). The h.f. and l.f. amplitude maxima coincide, therefore, at only a limited number of fixed poloidal positions. Because the h.f. mode decays very strongly away from the x-point of the l.f. island, these two effects can result in a standing wave pattern for the h.f. amplitude. Strong ballooning would cause this standing wave pattern to be observed only on the large major radius side.

3.1.2. Simulation of L.F. and H.F. Modes

With the phenomenological picture of the h.f. mode described in 3.1.1. as guidance, one can construct mathematical models of the l.f. and h.f. modes such that they simulate the experimental results of Fig. 3. This model has to incorporate the observed ballooning of both modes, and the poloidal decay of the h.f. mode amplitude away from the x-point of the $m_l=1/n_l=1$ island. The details of the model are described in the Appendix.

The results of the simulation are shown in Figs. 10 and 11. In Fig. 10, the experimental data (a), similar to Fig. 3, are compared to the simulation (b). The poloidal mode number is set to be $m_h=5$. The simulation duplicates the features of the experimental data. The simulation shows good agreement with the strength of ballooning of both modes, and agrees somewhat less with the poloidal decay rate (away from the x-point of the

$m_l=1/n_l=1$ island) of the h.f. mode. The stronger ballooning of the h.f. mode is also well simulated: at the top and bottom of a and b the maximum of the h.f. burst is shifted from the maximum toward the steep part of the l.f. trace. The phase velocities of the two modes and the phase relationship between the two modes are also correctly described in the simulation (broken lines l for l.f. - and h for h.f. in Fig. 10a and b).

The simulation of the poloidal structure (amplitude) of the h.f. mode for four characteristic time points in Fig. 10 (indicated by arrows and numbered 1 to 4) are shown in Fig. 11. The polar diagrams 1 and 2 describe the h.f. mode rotation of 90° when the x-point is at $\varphi=90°$ (1) and rotates by $\Delta\varphi=4.5°$(2). 1 and 2 show both the effect of the ballooning and the poloidal decay away from the x-point. The polar diagrams 3 and 4 show two extreme amplitudes of the h.f. mode caused by ballooning: 3 when the x-point of the l.f. island is at the midplane on the large major radius side ($\varphi=0°$), and 4 when the same x-point is at the midplane on the small major radius side ($\phi=180°$).

In this simulation it was assumed that the profile jaggedness is not caused by the constructive and destructive interference of two diode line-of-sight contributions from the perturbed shell. Instead, it was assumed to be a result of the poloidal standing wave pattern on the large major radius side, as described in the Section 3.1.1. To determine which of the two assumptions explains the profile jaggedness further measurements with a diode array orthogonal to the present soft x-ray system are planned.

The simulation demonstrates that the data support a ballooning structure for both modes, and the poloidal decay of the h.f. mode away from the x-point of the l.f. island. In addition, it gives a rough quantitative estimate for both effects.

3.1.3. Effect of Higher L.F. Harmonics On H.F. Mode

The effect of the higher harmonics of the $m_l=1/n_l=1$ mode, and the role these harmonics play in the excitation of the h.f. modes, remain unclear. The high harmonics of $m_l=1/n_l=1$ are normally very strong for the conditions where the h.f. bursting is strong, and they thereby create higher order non-axisymmetric equilibria. If the non-axisymmetric equilibrium of the $m_l=1/n_l=1$ island excites the h.f. modes, so should the higher harmonics with their non-axisymmetric equilibria.

In addition to the "light-house" effect caused by the fundamental of the l.f. mode, the higher harmonics of the low frequency mode should contribute to the observed spectral peaks. This will occur through the nonlinear interaction between the harmonics of the low frequency mode, $l\omega_l/lm_l/ln_l$, and the high frequency mode, $\omega_h/m_h/n_h$. This means that a

part of the amplitude of the high frequency peaks is due to the additional, real high frequency modes, $\omega_h \pm l\omega_l$ / $m_h \pm lm_l$ / $n_h \pm ln_l$, with l=2, 3 ... obtained through a nonlinear interaction with the second (l=2), third (l=3), etc. harmonic of the l.f. mode. This kind of non-linear interaction of modes of different n has been observed on PBX-M.[9] Note that k and l are not the same integers: k describes the "light-house" effect of the h.f. mode and l the higher harmonics of the l.f. mode. This effect is weak and hard to detect, even for the first l.f. harmonic l=2. There is, however, a possible indication that the second harmonic (m_l=2/n_l=2) does excite a weak h.f. mode, with two bursts of the h.f. mode during one period of the m_l=1/n_l=1 mode.

Finally, the frequency of the h.f. mode is found to be equal or very close to the frequency of one of the higher harmonics of the l.f. mode, $\omega_h = 15\omega_l$. The reason is not understood, but it is an indication of interaction of the higher harmonics of the l.f. mode with the h.f. mode.

3.2. H.F. Mode in Weakly Non-Axisymmetric and Axisymmetric Configuration

3.2.1. Weakly Non-Axisymmetric Case

A strong non-axisymmetric equilibrium is not a necessary condition for the excitation of the h.f. modes. In a much weaker m_l=1/n_l=1 non-axisymmetric equilibrium, having an m_l=1/n_l=1 island with a normalized maximum modulation of only 0.9% and a width of about w_{midl1} = 0.4 cm at r_{midl1} = 14 cm, the h.f. mode was again modulated by the l.f. mode. However, the damping in the poloidal direction away from the m_l=1/n_l=1 island x-point was weaker in this case, and the h.f. mode amplitude was smaller even at the o-side of the island. This was observed during the β-saturation period, where the n_l=1 global mode was still weak. A strong n=3 mode was also observed in the central part of the plasma, but it did not show any effect on the h.f. mode. A possible reason for this might be that m_l=5(?)/n_l=3 islands were too far from the h.f. mode to influence it.

3.2.2. Axisymmetric Case

We have also observed cases of a continuous, non-bursting h.f. mode with no presence of any l.f. mode, i.e., the equilibrium was axisymmetric (Fig. 12). This h.f. mode also shows a preferred poloidal rotation in the top-to-bottom direction (see Fig. 12), indicating that only the perturbation peak on the large major radius side is observed, and

none on the small major radius side. This supports the ballooning character of these modes.

These cases were observed early in the neutral beam heating phase, where β is still increasing (β_{tor} = 0.018 or lower and β_{pol} = 1.5), or after one of four neutral beams has been switched off. The amplitude profiles of the two h.f. peaks at 97 and 114 are shown in Fig. 13. The profiles of the two other peaks at 140 and 166 kHz are not shown. These profiles are very similar to the profiles of the bursting h.f. mode of Fig. 5, and the same comments on the m_h-number of the mode (between 4 and 6 at 114 kHz) on a narrow shell also apply. The 97 kHz mode seems to be independent of the other three modes, and unlike the others, it eventually disappears. The frequency gap of 26 kHz between the other three modes is not understood, because the m_l=1/n_l=1 mode has a 15 kHz frequency just a few ms earlier. Comparison of the m_l=1/n_l=1 amplitude profile (trace L) with the h.f. mode profiles of Fig. 13 (traces H1 and H2) suggests that the h.f. mode is localized either on or close to the q=1 surface. From the top-to-bottom phase change and the mode location on the q=1 surface, the m- and n-numbers are given by m_h=5 or 6 and n_h=5 or 6. Simulation of this mode under the assumption of somewhat weaker ballooning, and with m- and n-numbers m_h=5/n_h=5, is shown in Figs 12B and 14. The simulation duplicates the features of the measurements, thus supporing the model.

These modes have all of the characteristics of the bursting, non-axisymmetric h.f. modes (Figs. 3 to 7), so they must have the same physical origin.

These two examples of h.f. modes show that, although the bursting, non-axisymmetric h.f. modes are prevalent in PBX-M, the existence of a non-axisymmetric equilibrium (a strong m_l=1/n_l=1 island) is not a necessary condition for the excitation of the h.f. modes.

4. DISCUSSION

The obvious question is which instability causes this perturbation. One class of instabilities which could be at work here would involve high energy particles with high parallel velocities. In our case, they are the neutral beam particles. The instability will be more readily identified by performing experiments where the relevant plasma parameters are changed. All the data for the present work were obtained under the same plasma parameter conditions: neither the toroidal magnetic field nor the plasma density varied substantially. In future work these conditions will be varied. Because this mode is observed only in high-β discharges, the mode is obviously connected to either the pressure or the pressure gradient. There are three such possibilities: the toroidicity-induced shear

Alfvén eigenmode (TAE) [13,14,15,16,17,18,19] or its derivative EAE (Ellipticity-induced Alfvén Eigenmode) [20], the kinetic ballooning mode (KBM) [13,21,22], or the ideal ballooning mode [22].

In cylindrical geometry, shear Alfvén continua can exist with toroidal and poloidal mode numbers m/n and (m+1)/n, i.e., if they satisfy the Alfvén resonance condition $\omega=k_{\|}v_A$, where v_A is the Alfvén velocity, $v_A=B/(4\pi m_i n_i)^{1/2}$. These continua intersect at the radial position r_o, defined by $q_o(r_o)=(2m+1)/2n$. In toroidal geometry this degeneracy is resolved with a gap, where all the frequencies are forbidden except for those constituting the TAE mode. Earlier it was believed that the TAE mode can be excited with fast circulating ions only if the injection parallel velocity, $v_{\|}$, satisfies the condition $v_{\|}\geq v_A$. Biglari et al have shown that there is another resonance at $1/3v_A$, so that the general condition is now $v_{\|}\geq 1/3v_A$.

The real frequency of these modes is given by $\omega_r\approx 1/2\ \omega_A$, where $\omega_A\approx v_A/2q_oR$ is the TAE frequency with $q_o=(2m+1)/2n$. For the growth rate of the TAE-mode, we will use two expressions. One is given by Fu and Van Dam [16]:

$$\gamma/\omega_r=9/4\{\beta_h(\omega^*_h/\omega_r-1/2)F-\beta_e v_A/v_{Te}\},$$

where β_h is the beta of fast, circulating ions, $\omega^*_h=m/r\ (\rho_i v_h)/L_{ph}$ is the diamagnetic frequency for an average fast ion, $(L_{ph})-1=d(\ln p_{ih})/dr$ is the pressure scale length for the fast ions, $F=(1+2x^2+2x^4)\exp(-x^2)$ with $x=v_A/v_{\|}$, β_e is the electron pressure, and v_e is the electron thermal velocity.

The other expression for the TAE mode and (with $v_{\|}\geq v_A$) is given by Biglari et al [19]:

$$\gamma/\omega_r\approx(\pi q^2/3)\ k_\theta\rho_h\beta_h(R/L_{ph})[1-3/(2qk_\theta\rho_h)\ (v_A/v_m)\ (L_{ph}/R)],$$

where v_m is the maximum injection velocity and 'h' denotes highly energetic component. For lower fast ion energies, where $v_A>v_{\|m}>v_A/3$, the above growth rate is reduced by a factor of 3^4.

According to Biglari and Chen [22], the expression for the real frequency of the KBM mode for the case of the wave-transit ion resonance is $\omega_r=\omega^*_{ip}$, where ω^*_{ip} is the diamagnetic frequency of the thermal ions. The growth rate is given by:

$$\gamma/\omega r\approx\pi^2/16\ q_o^2\ \varepsilon^{-3/2}\ \beta_h\ (\omega_A/\omega_{tm})^2\ \{(\omega^*_{ip}\omega^*_{pm})/(3\ \omega_{tm}^2)-2\varepsilon\},$$

where ε is the local inverse aspect ratio, $\omega_{tm} = v_{\|m}/2q_oR$ and $\omega^*_{pm}=m/r\ (\rho_m v_{\|m})/L_{pm}$ is the diamagnetic frequency of the fast ions of energy equal to the beam injection energy.

The comparison of the values of the real frequencies and the growth rates for both expressions for the TAE-mode and for the KBM-mode are shown in Table II. The plasma parameters for which these high-frequency bursts appear are either obtained directly from the measurements or indirectly from the TRANSP code calculations based on the measured plasma profiles. The values of the most important parameters are as follows: ion density $n_i=2.5\times10^{13}$ cm^{-3}, ion temperature $T_i=2$ keV, toroidal field B=1.3 T, neutral beam injection energy $E_m=42$ keV, inverse aspect ratio $\varepsilon=0.09$, relative fast ion pressure $\beta_h=0.005$, and scale lengths of the thermal and fast ions $L_{pi}=L_{ph}=L_{pm}=15$ cm. Following the previous discussion of possible m and n numbers, we assumed an $m_h=5/n_h=5$ mode for the 110 kHz peak of Fig. 5.

The theoretical estimates for the real frequencies are compared to the measured frequency, including its Doppler-shifted value (f_l). This value is estimated from the value of the low frequency, f_l, using relation $f_h=f_m-n_h\ f_l$. The theoretical values for the TAE-mode and the KBM-mode are both close to the measured values, so the real frequency alone cannot distinguish which mode is responsible.

The Biglari theoretical values for the growth rates of the TAE-mode and KBM-mode are very close. The growth rate according to Fu & van Damm is quite different, but their formula is valid only for $v_{\|}>v_A$. If we divide the Fu & Van Damm value by the same factor 3^4 as in the case of Biglari et al., the resultant value of the growth rate is almost identical to the Biglari et al value, 2.2×10^4, showing that the two formulae are consistent. Unfortunately, the experimental value of the growth rate is difficult to estimate because of the bursting nature of the high frequency signal; therefore, a comparison between the theoretical and the experimental values of the growth rates is not possible.

The conclusion from Table II is that either of these modes could be responsible for the high-frequency bursting, and further studies, possibly involving the scanning of different plasma parameters, need to be made in order to decide which mode is responsible. However, there is one difficulty with the TAE explanation. TAE modes are global modes, and are predicted to be localized in the gaps $q_o=(2m+1)/(2n)$ between two modes m and m+1. The experimental results show that the h.f. mode is never localized between two rational surfaces of low rational number (e.g., q=1 and q=2). Instead, they are either exactly on a rational surface or close to it.

Hegna and Callen in their paper show that the stability properties of the ideal ballooning modes are altered on the magnetic surface closest to the x point of the magnetic island. They also show that the eigenfunctions localized near the x point and on the bad curvature side of the tokamak are more susceptible to the ballooning instability, because the stabilizing effect of the field-line bending is reduced there. They also believe that, because of this presence of a strong m=1 island preceding the sawtooth crash, the secondary ballooning instabilities might play a role in the crash phase of the sawteeth. Our observations agree very well with the Hegna and Callen model of non-axisymmetric excitation of the h.f. mode, except that they treat the case of an ideal ballooning mode, while we obviously see an instability primarily involving the fast ions.

The discharges described in this paper were investigated for their ideal ballooning mode stability during the discharge period with high-β_{pol} and before the β-collapse. It was found that in a rather large volume of the central part of the discharge, where $q<2.5$, the plasma is normally close to the first stability limit. This is shown in Fig. 15, where on the S-α diagram for several values of q, the actual pressure gradient and shear found in the discharge are represented by a point indicated in the figure. The shear and pressure gradient parameters are defined as $S(\psi)=(2v/q)(dq/d\psi)(d\psi/dv)$ and $\alpha(\psi)=(-2\mu_0)(dp/d\psi)(dv/d\psi)(v/2\pi^2R)^{-1/2}$, where p, v, and R are the pressure, volume, and the major radius defined by the flux ψ, and ψ is the poloidal flux.

It is clear that for the part of the discharge where the high frequency modes are found, the plasma conditions are near the stability boundary for ideal ballooning. It is conceivable that the additional term due to the non-axisymmetric equilibrium driving the ballooning instability could bring the central plasma into the ballooning unstable region. The central plasma is almost unstable for the ballooning modes, and even if the observed h.f. modes were not ideal ballooning modes, we should expect KBM modes because of the large fast particle β. The rather large loss of fast particles, compared to the thermal energy loss, argues for either a KBM mode or a TAE mode modified by the high β.

In this paper we did not address the possibility of other modes connected with the TAE modes, like ellipticity- and triangularity-induced Alfvén eigenmodes (EAE) or kinetic toroidal Alfvén eigenmodes (KTAE). The appropriate damping mechanism for the modes observed in PBX-M plasmas is also uncertain for the same reason that we cannot determine whether the modes observed are TAE or KBM modes. Future plasma parameter studies are needed to clarify these issues.

4. APPENDIX

Simulation of L.F. and H.F. Modes

A) Using a thin shell approximation, the time evolution of the l.f. and h.f. modes are simulated with the following functions

a) for the l.f. mode:

$$S_l(t, \phi) = A_l \{\exp[B_l [\cos(90^o - \chi_1)-1]] \exp[C_l [\cos(\omega_l t - \chi_1)-1]] \cos(\omega_l t - \chi_1) + \exp[B_l [\cos(90^o + \chi_1)-1]] \exp[C_l [\cos(\omega_l t + \chi_1)-1]] \cos(\omega_l t + \chi_1)\}$$

b) for the h.f. mode:

$$S_h(t, \phi) = A_h \{\exp[B_h [\cos(90^o - \chi_1)-1]] \exp[C_h [\cos(\omega_l t - \chi_1)-1]] \cos[\omega_h t - m_h \chi_1] + \exp[B_h [\cos(90^o + \chi_1)-1]] \exp[C_h [\cos(\omega_l t + \chi_1)-1]] \cos[\omega_h t + m_h \chi_1].$$

The subscript l denotes the l.f. mode and h the h.f. mode. The other variables are as follows: $\chi_1=90^\circ-\varphi_d$, where φ_d is the poloidal position of the diode, ω_l and ω_h are the frequencies of the l.f. and the h.f. mode,and m_h is the poloidal mode number of the h.f. mode.

The constants B_l, C_l, B_h, and C_h are chosen to obtain the best agreement with experiment: B_l=0.7, C_l=0.2.5, B_h=2, and C_h=3. Note that the B_h and C_h values are larger than the corresponding values of B_l and C_l, reflecting the stronger ballooning of the h.f. mode. From experiment, $\omega_h=15\omega_l$. The first exponential simulates the ballooning effect and the second the decay away from the x-point. The two additive terms in the expressions for S_l and S_h represent the mode on the large and small major radius sides. The h.f. mode ballooning is much stronger.

B) The polar plot of the amplitude of the l.f. and h.f. mode (as a function of the poloidal angle φ) is represented by the following functions:

a) for the l.f. mode:

$$S_l(\varphi,\varphi_x) = 1 + A_l \exp(B_l \cos\varphi) \exp[C_l \cos(\varphi - \varphi_x)] \cos(\varphi - \varphi_x)$$

b) for the h.f. mode:

$$S_h(\varphi, \varphi_x, \phi_h) = 1 + A_h \exp(B_h \cos\varphi) \exp[C_h \cos(\varphi - \varphi_x)] \cos[m_h(\varphi - \varphi_x) - \varphi_h].$$

Here φ_x is the poloidal position of the x-point of the $m_l=1/n_l=1$ island, and φ_h is the arbitrary phase of the h.f. mode.

Acknowledgements:

The authors would like to thank K.L. Wong, E.J. Strait, H. Biglari, and G.Y. Fu for many helpful discussions. This work was supported by the US DoE Contract No. DE-AC02-76-CHO-3037.

(a) ARACOR, Sunnyvale, CA
(b) JT-60U, Jaeri, Tokai-mura, Ibaraki-ken, Naka-gun, Japan
(c) Laboratoire pour l'Armenment, Berne, Switzerland
(d) Department of Nuclear Engineering, University of Wisconsin, Madison, WI, USA
(e) Grumman Aerospace Corporation, Bethpage, NY, USA
(f) 72 Jacobs Creek Rd., West Trenton, NJ, USA
(g) Institute of Plasma Physics, Hefei, China
(h) Fusion Physics & Technology, Torrance, CA, USA
(i) University of California, Lawrence Livermore National Laboratory, Livermore, CA, USA
(j) Southwestern Institute of Physics, Leshan, China

REFERENCES:

[1] BELL, R.E., ASAKURA, N., BERNABEI, S., et al., Phys. Fluids B **2**, 1271 (1990).

[2] SAUTHOFF, S., ASAKURA, N., BELL, R., et al., Proceedings of the 13th Intern. Conf. on Plasma Phys. and Contr. Nucl. Fus. Research, (Washington, DC, October 1990), (IAEA, Vienna, Austria) Vol. I, 709 (1991).

[3] WONG, K.L., FONCK, R.J., PAUL, S.F., et al., Phys. Rev. Lett. **66**, 1874 (1991).

[4] DURST, R.D., FONCK, R.J., WONG, K.L., CHENG, C.Z., FREDRICKSON, E.D., and PAUL, S.F., Phys. Fluids B **4**, 3707 (1992).

[5] HEIDBRINK, W.W., STRAIT, E.J., DOYLE, E., SAGER, G., SNIDER, R.T., Nucl. Fusion **31**, 1635 (1991).

[6] STRAIT, E.J., HEIDBRINK, W.W., CHU, M.S., DUONG, H.H., LAO, L.L., TURNBULL, A.D., and the DIII-D Team, 14th International Conference on Plasma Physics and Controlled Nuclear Fusion, Würzburg, September/October 1992, paper IAEA CN-56/D-3-3.

[7] HEIDBRINK, W.W., BOL, K., BUCHENAUER, et al., Phys. Rev. Lett. **57**, 835 (1986).

[8] NAGAYAMA, Y., SABBAGH, S.A., MANICKAM, J., et al., Phys. Rev. Lett. **69**, 2376 (1992).

[9] SESNIC, S., KAYE, S., and OKABAYASHI, M., Proceedings of the 18th European Conference on Controlled Fusion and Plasma Physics, Berlin, 3-7 June, 1991; Europhysics Conference Abstracts, V. 15 C, Part II, p.1197.

[10] LEVINTON, F., FONCK, R., GAMMEL, G.M., et al., Phys. Rev. Lett. **63**, 2060 (1989).

[11] KUGEL, H.W., GAMMEL, G.M., KAITA, R.,. REUSCH, M.F, and ROBERTS, D.W., Rev. Sci. Instrum. **59**, 1635 (1988).

[12] HEIDBRINK, W.W., Rev. Sci. Instrum. **57**, 1769 (1986).

13. CHEN, L. in Theory of Fusion Plasmas, Ed. J. Vaclavik, F. Troyon, and E. Sindoni (CRPP, Association EURATOM, 1988), p. 327.

[14] CHENG, C.Z., CHENG, L., and CHANCE, M.S., Ann. Phys. **161**, 21 (1985).

[15] CHENG, C.Z. and CHANCE, M.S., Phys. Fluids **29**, 3695 (1986).

[16] FU, G.Y and VAN DAM, J.W., Phys. Fluids B **1**, 1949 (1989).

[17] CHENG, C.Z., Phys. Fluids B **2**, 1427 (1990).

[18] FU, G.F. and CHENG, C.Z., Phys. Fluids B **2**, 985 (1990).

[19] BIGLARI, H., ZONCA, F., and CHEN, L., Phys. Fluids B **4**, 2385 (1992).

[20] VILLARD, L., FU, G.Y, Nucl. Fusion **32**, 1695 (1992).

[21] TANG, W.M., CONNOR, J.W., and HASTIE, R.J., Nucl. Fusion **20**, 1439 (1980).

[22] BIGLARI, H. and CHEN, L., to be published in Phys. Rev. Lett., PPPL-2790.

[23] HEGNA, C.C. and CALLEN, J.D., Phys. Fluids B **4**, 3031 (1992).

FIGURE CAPTIONS

Fig. 1. Equilibrium magnetic surfaces for a discharge with the h.f. mode described in this paper. The lines-of-sight of individual soft x-ray diodes, used in the MHD analysis of the h.f. mode, are also shown. Position of a given diode, z, is defined as the vertical height from the midplane to the intersection between the diode line-of-sight and a vertical line at R=165 cm.

Fig. 2. Temporal evolution of representative plasma parameters in a typical high-β_{pol} discharge: toroidal beta, β_{tor}; electron density, n_e; soft x-ray signals along center, off-axis, and edge chords, I_x; H_α signal, I_H; and neutral beam injection power, P_b. Toroidal beta shows several distinct periods during the discharge: β-rise (from 410 to 460 ms and 490 to 510 ms), β-saturation (from 460 to 490 ms and 510 to 535 ms) and β-collapse (after 535 ms).

Fig. 3. Soft x-ray intensity signals in central part of plasma, with high pass filter of 0.5 kHz (full line) or 90 kHz (broken line). The scale for the h.f. signals is a factor of 10 higher than the l.f. signals. The two lines labeled *l.f. max* and *h.f. max* follow the l.f. amplitude and the h.f. burst envelope maxima, respectively, from top to bottom. Their offsets indicate a time shift between the two maxima. Broken lines indicate top-to-bottom (t/b) propagation of the larger l.f. peak at the large major radius side, and the bottom-to-top (b/t) propagation of the smaller peak on the small major radius side.

Fig. 4. Power spectra of high frequency bursts in SX radiation. The regularly-spaced high frequency peaks occur between 100 and 160 kHz, and they are separated by the frequency of the low frequency mode (7.3 kHz). The broken straight line represents the estimated photon noise.

Fig. 5. Power spectrum profiles of the successive peaks at 103, 110, 118, and 128 kHz (Fig. 3). Modes are localized inside z=20 cm. Curve Ph represents calculated photon noise.

Fig. 6. Normalized power spectrum of the n=1 mode (L.F.), three consecutive h.f. modes (H.F.), and calculated photon noise (Ph). Three consecutive h.f. modes are at 96 (curve a), 103 (curve b), and 110 (curve c) kHz.

Fig. 7. a) Phase profiles of five successive high frequency peaks (96, 103, 110, 118 and 125 kHz) in Fig. 4. b) Phase profiles of the l.f. m=1/n=1 mode and its four successive harmonics: m=2/n=2, 3/3, 4/4, and 5/5.

Fig. 8. Correlation between the h.f. mode and the neutron rate drop.

a) central soft x-ray diode signal showing strong n=1 activity;

b) signal of the same diode but digitally filtered by a high pass filter of 60 kHz. High peaks correspond to h.f. bursts.

c) Neutron signal digitally filtered by a low pass filter of 4 kHz.

d) Three soft x-ray signals at three different radial positions digitally filtered by a low pass filter of 4 kHz.

Fig. 9. Normalized profile change during an h.f. burst in soft x-ray radiation. $\Delta I_x = I_x - I_{xo}$, where I_{xo} and I_x are the intensities at the beginning and at the end of the h.f. burst.

Fig. 10. Comparison of the experimental data (a) with the simulation (b) for the l.f. (solid line) and h.f. (broken lines) modes. Broken straight lines denoted by l and h are lines of constant phase for the l.f. (line l) and h.f. (line h) modes.

Fig. 11. Polar plot simulation of the amplitude of the h.f. bursting mode for four different times during one rotation in the poloidal direction (angle φ). The plots 1 to 4 correspond to times in Fig.10B denoted by arrows labeled 1 to 4. The angular constants φ_x and φ_h are defined in Appendix.

Fig. 12. Continuous h.f. mode in axisymmetric equilibrium (no m=1/n=1 island): Soft x-ray signals digitally filtered with 90 kHz high pass filter at several radial positions: the broken sloped line indicates a continuous change in phase from the top to the bottom diode and, therefore, a preferential direction in poloidal phase velocity ("ballooning"). Part B: Simulation shows, that ballooning and m_h=5 correctly describe the observed mode.

Fig 13. a) Power spectrum profiles for continuous h.f. modes at 97 (H2), 114 (H1), and l.f. mode (L). Trace Ph represents the estimated photon noise.

Fig.14. Polar plot simulation of the amplitude of the h.f. continuous mode for four

different times over one h.f. cycle.

Fig.15. S-α diagram showing ideal ballooning mode stability limits for a typical high β_{pol} discharge at several values of q. Solid squares represent actual experimental equilibria, and the central values are close to the stability limit. Pressure and q profile. are also shown.

Table I

Frequency peaks of the h.f. mode with corresponding m/n values

	f [kHz]	95	103	110	118	125	....
TAE	(2m+1)/2n	7/6	9/8	11/10	13/12	15/14	
S	m/n	3/3	4/4	5/5	6/6	7/7	....
M	m/n	3/2	4/3	5/4	6/5	7/6	....

Table II

Comparison of Theory and Measurement
(For m=5/n=5 and n_i=2.5x10^{13})

	TAE Mode		KBM	Measured	
	Fu & van Damm	Biglari et al.	Biglari et al	f_{meas} [kHz]	$f_{hf}=f_{meas}-nf_o$ [kHz]
Real frequency f_r [kHz]	84	84	68	118	73
Growth rate γ [s^{-1}]	$1.8x10^6$	$2.3x10^4$ *	$4.3x10^3$	$>10^4$	-

* without $1/(3)^4$: $1.9x10^6$

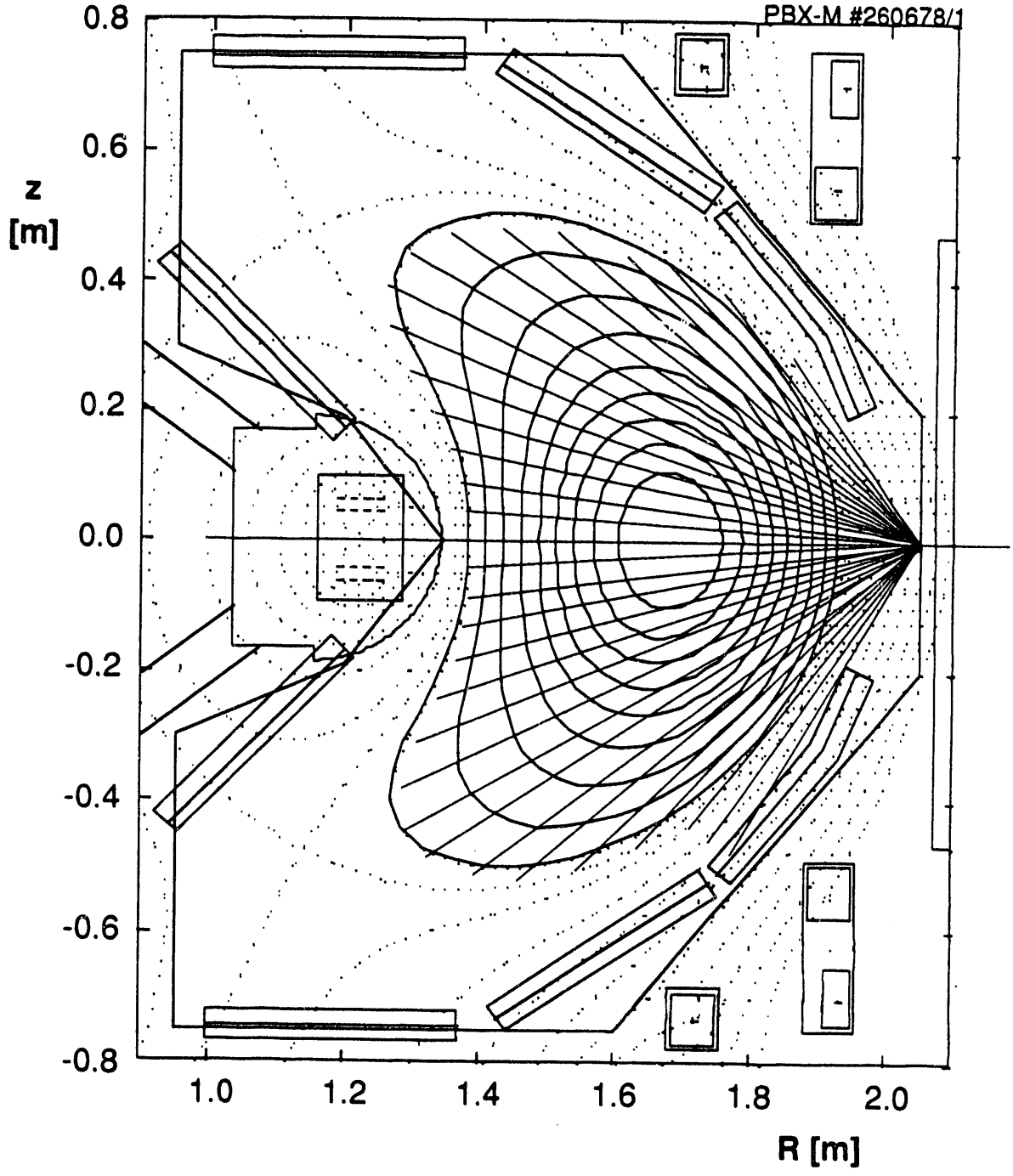

Fig. 1

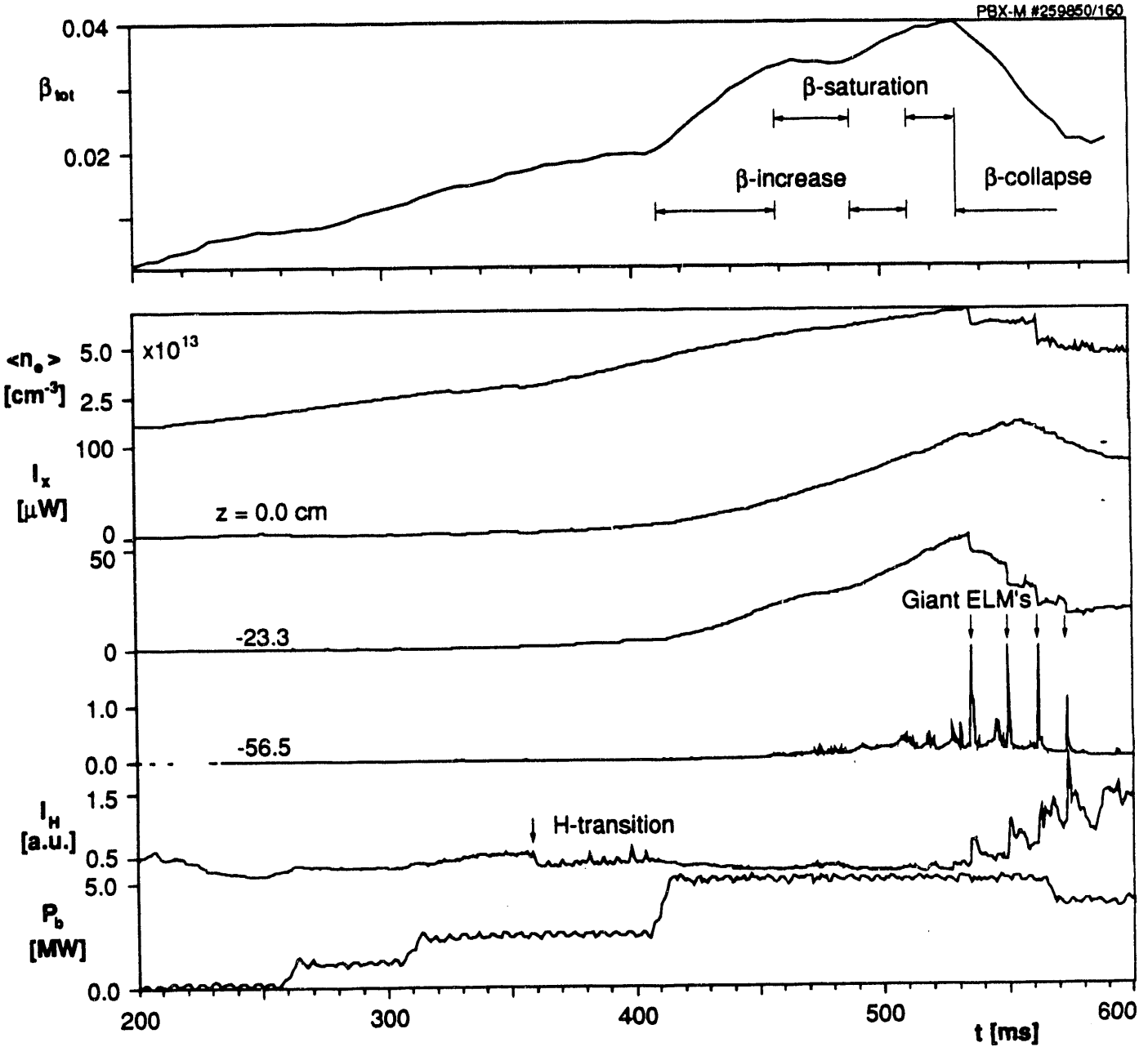
PBX-M #259850/160
0.04
β_{tot}
0.02
β-saturation
β-increase
β-collapse
$<n_e>$ [cm^{-3}]
5.0
x10^{13}
2.5
100
I_x [μW]
z = 0.0 cm
0
50
Giant ELM's
-23.3
0
1.0
-56.5
0.0
1.5
I_H [a.u.]
H-transition
0.5
5.0
P_b [MW]
0.0
200
300
400
500
600
t [ms]

Fig. 2

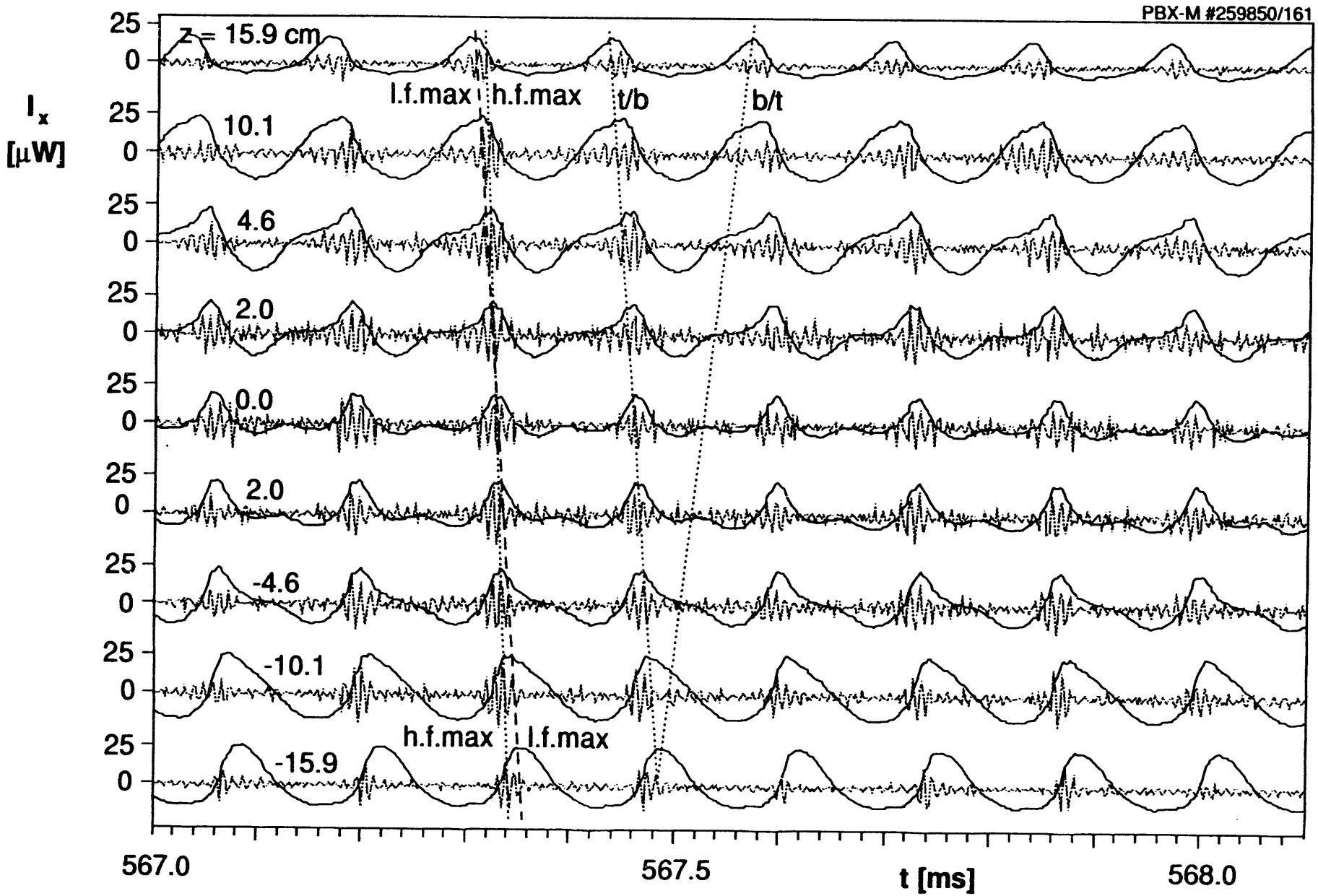
PBX-M #259850/161
I_x [μW]
z = 15.9 cm
10.1
4.6
2.0
0.0
2.0
-4.6
-10.1
-15.9
l.f.max
h.f.max
t/b
b/t
h.f.max
l.f.max
25
0
567.0
567.5
568.0
t [ms]

Fig. 3

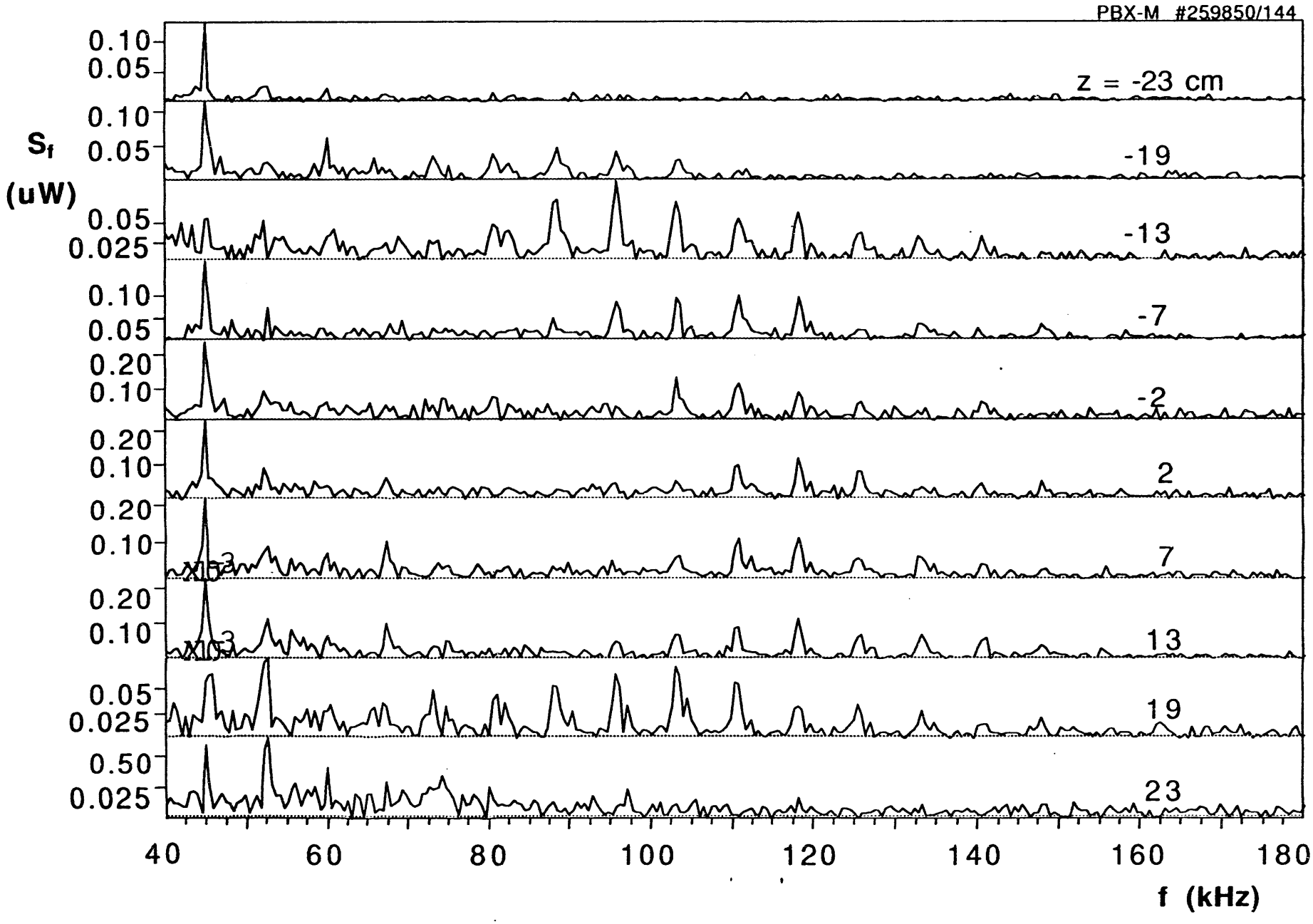
PBX-M #259850/144
S_f (uW)
z = -23 cm
-19
-13
-7
-2
2
7
13
19
23
0.10
0.05
0.025
0.20
0.50
x10^-3
40
60
80
100
120
140
160
180
f (kHz)

Fig. 4

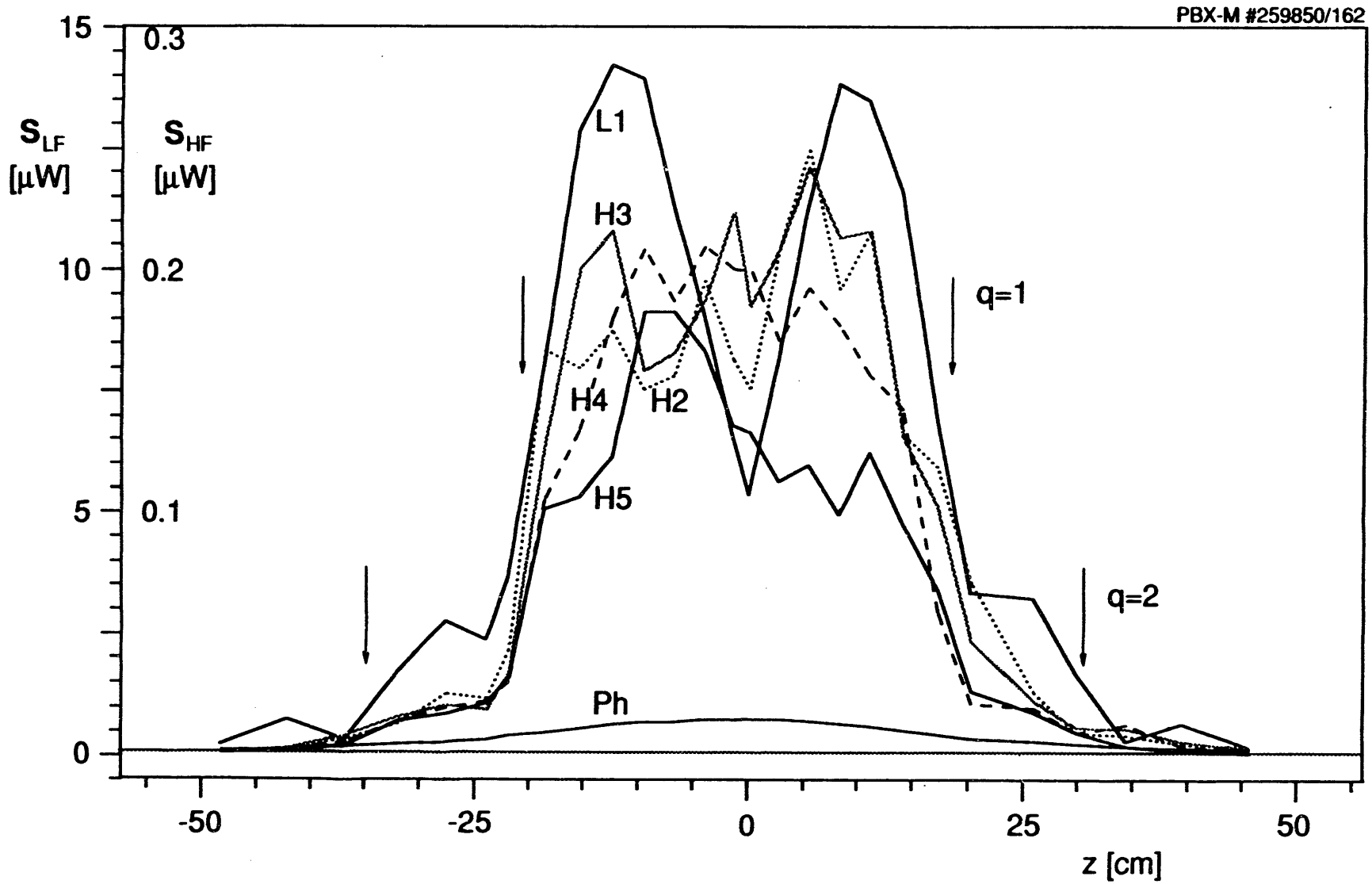
PBX-M #259850/162
S_{LF} [μW]
S_{HF} [μW]
15
10
5
0
0.3
0.2
0.1
L1
H3
H4
H2
H5
Ph
q=1
q=2
-50
-25
0
25
50
z [cm]

Fig. 6

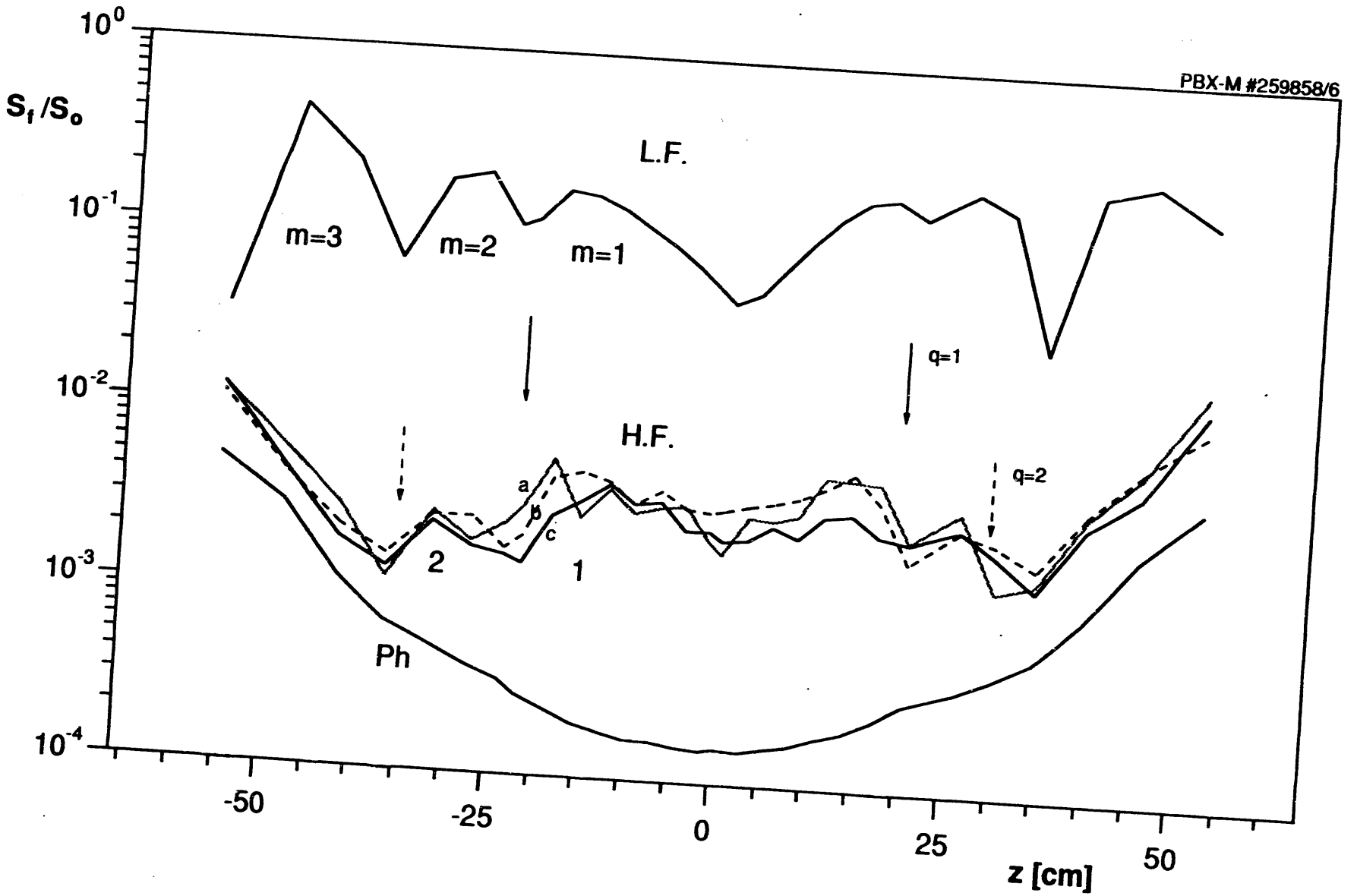
PBX-M #259858/6
S_f/S_o
10^0
10^{-1}
10^{-2}
10^{-3}
10^{-4}
L.F.
m=3
m=2
m=1
q=1
H.F.
q=2
a
b
c
2
1
Ph
-50
-25
0
25
50
z [cm]

Fig. 6

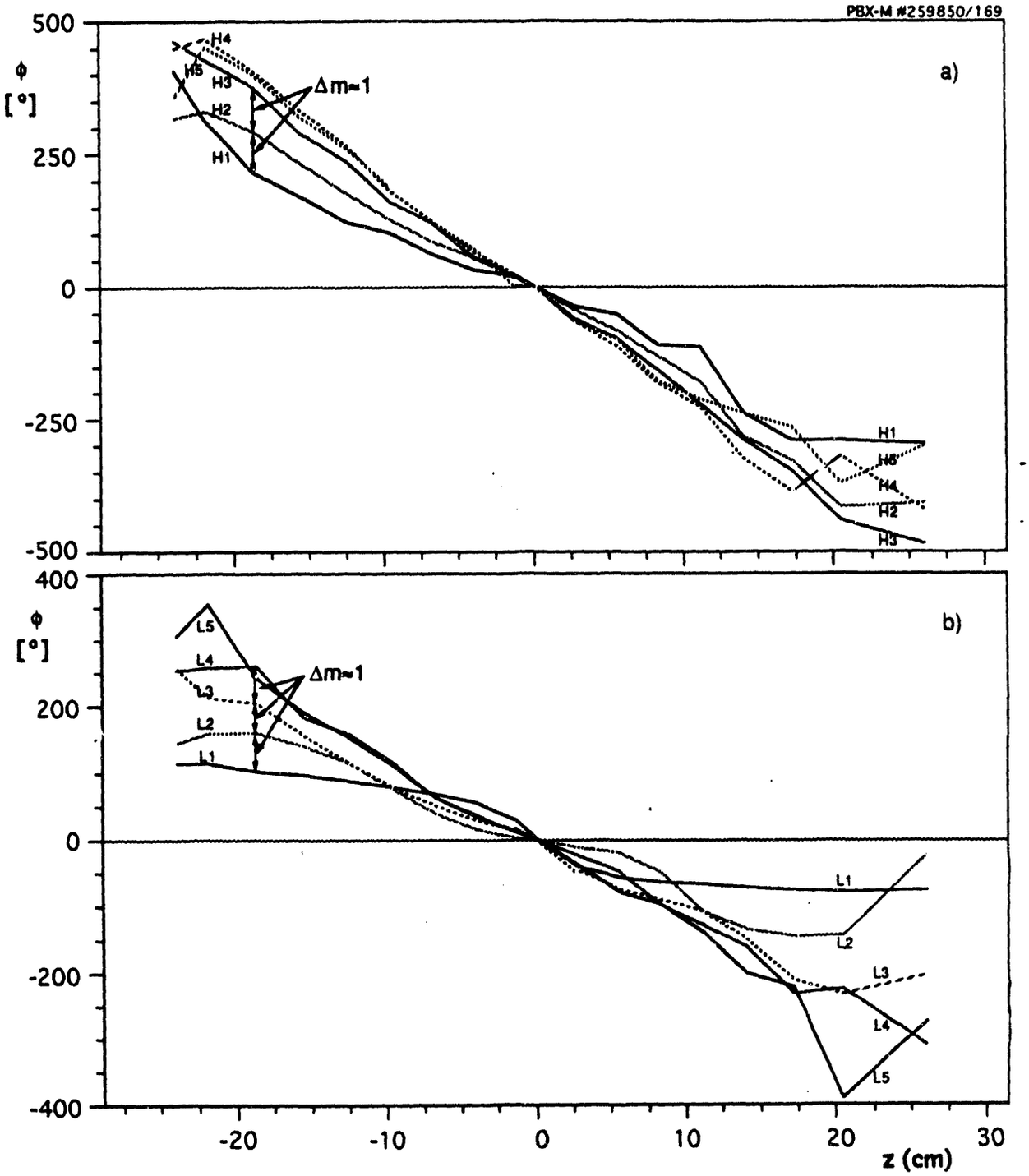
PBX-M #259850/169
a)
b)
φ
[°]
Δm≈1
H1
H2
H3
H4
H5
L1
L2
L3
L4
L5
500
250
0
-250
-500
400
200
-200
-400
-20
-10
0
10
20
30
z (cm)

Fig. 7

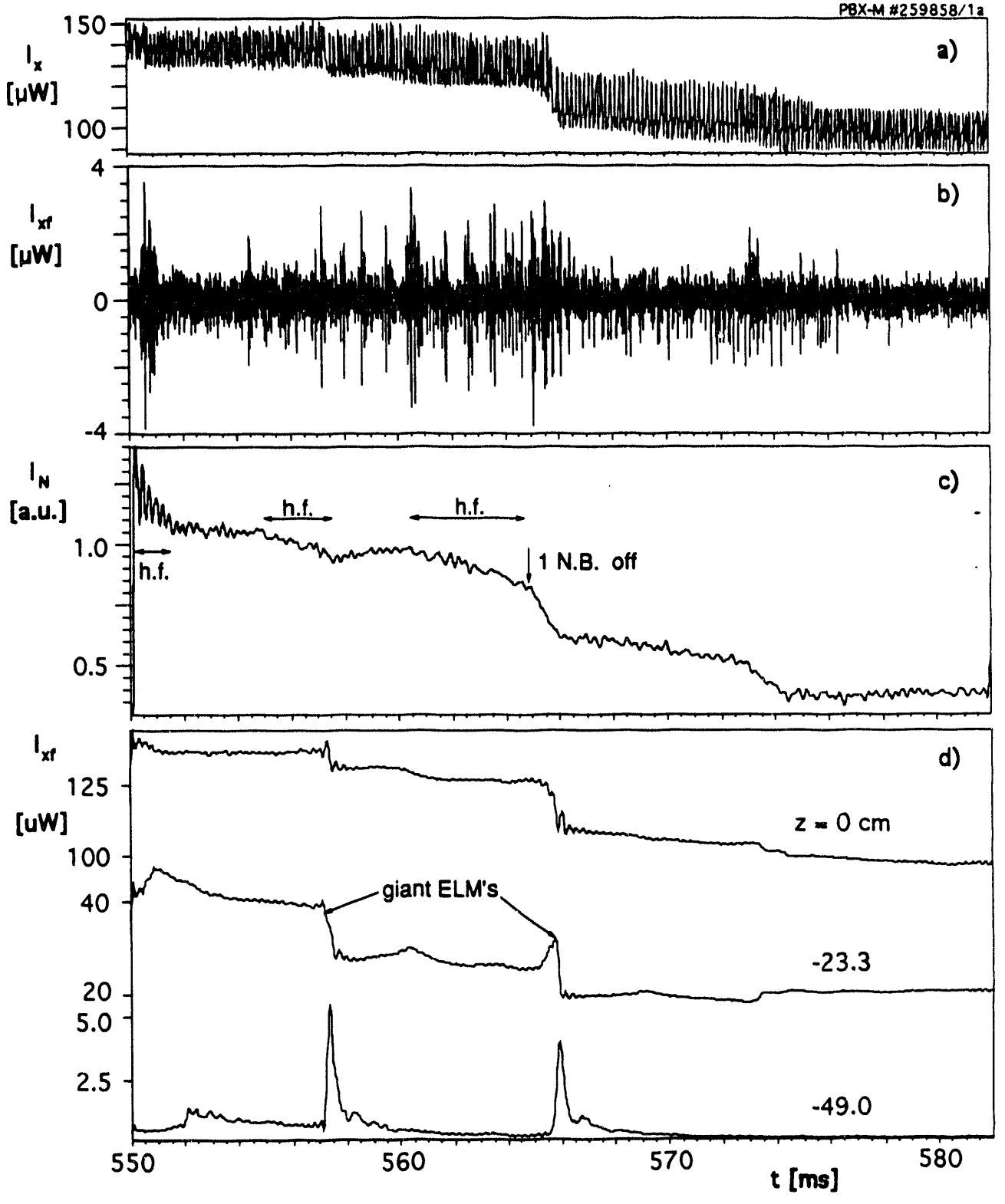
PBX-M #259858/1a
a)
I_x [μW]
150
100
b)
I_{xf} [μW]
4
0
-4
c)
I_N [a.u.]
1.0
0.5
h.f.
h.f.
h.f.
1 N.B. off
d)
I_{xf} [uW]
125
100
40
20
5.0
2.5
z = 0 cm
giant ELM's
-23.3
-49.0
550
560
570
580
t [ms]

Fig. 8

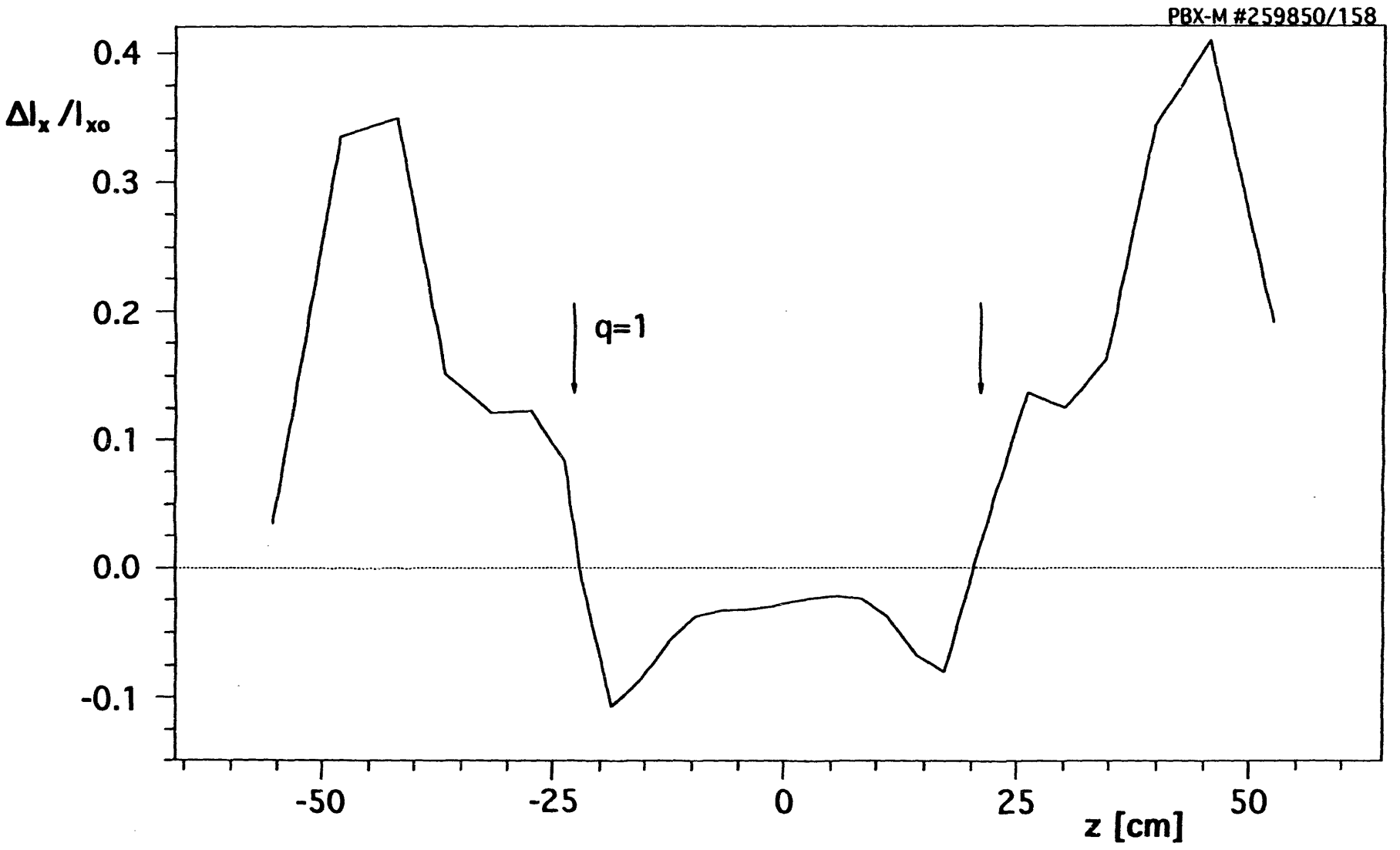
PBX-M #259850/158
0.4
0.3
0.2
0.1
0.0
-0.1
$\Delta I_x / I_{xo}$
q=1
-50
-25
0
25
50
z [cm]

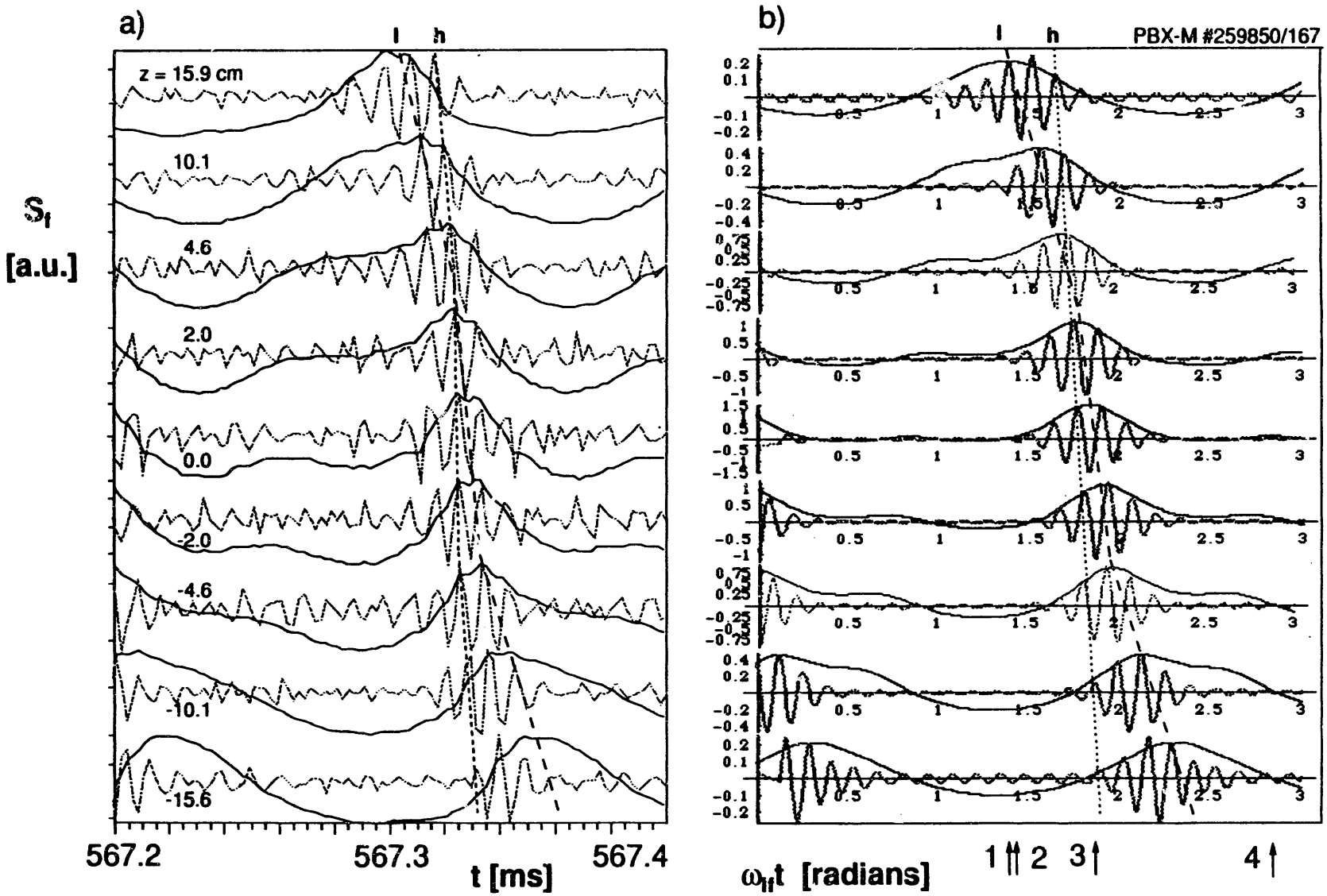
a)
b)
l
h
PBX-M #259850/167
z = 15.9 cm
10.1
4.6
2.0
0.0
-2.0
-4.6
-10.1
-15.6
S_f
[a.u.]
567.2
567.3
567.4
t [ms]
$\omega_{lf}t$ [radians]
1
2
3
4

Fig. 10

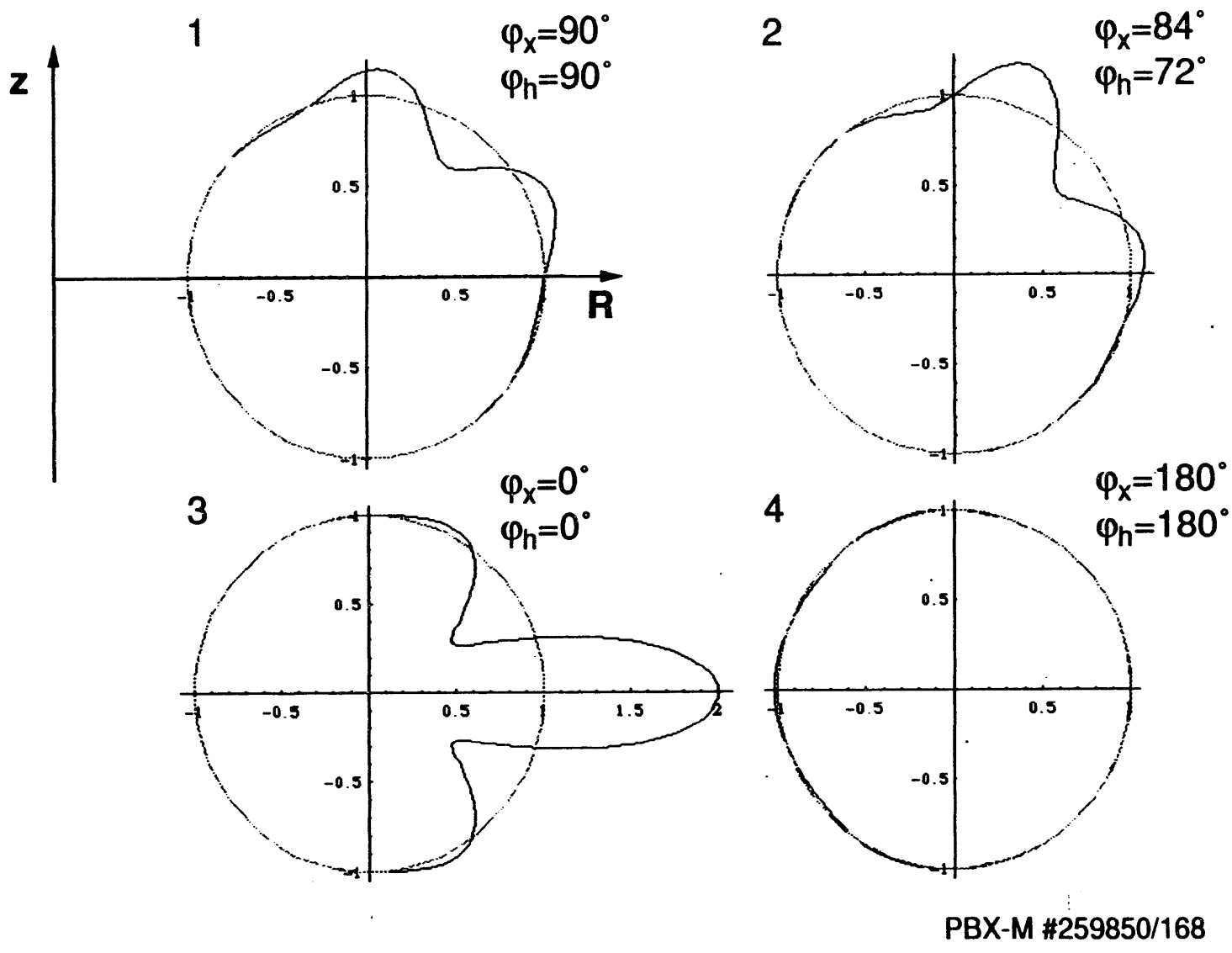
1
φ_x=90°
φ_h=90°
2
φ_x=84°
φ_h=72°
3
φ_x=0°
φ_h=0°
4
φ_x=180°
φ_h=180°
Z
R
-1
-0.5
0.5
1
1.5
2
PBX-M #259850/168

Fig. 11

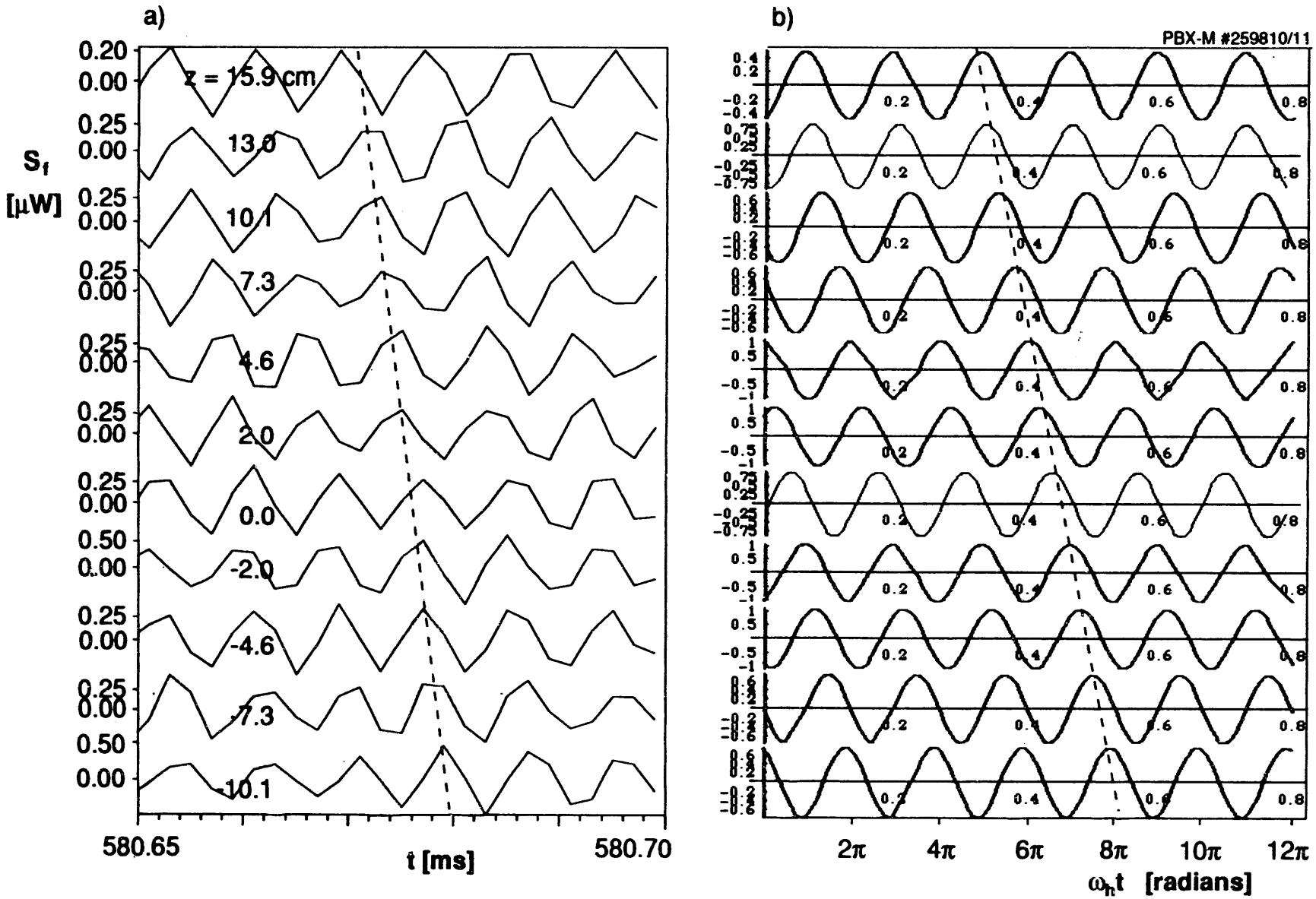
a)
b)
PBX-M #259810/11
S_f
[μW]
z = 15.9 cm
13.0
10.1
7.3
4.6
2.0
0.0
-2.0
-4.6
-7.3
-10.1
580.65
580.70
t [ms]
2π
4π
6π
8π
10π
12π
$\omega_h t$ [radians]

Fig. 12

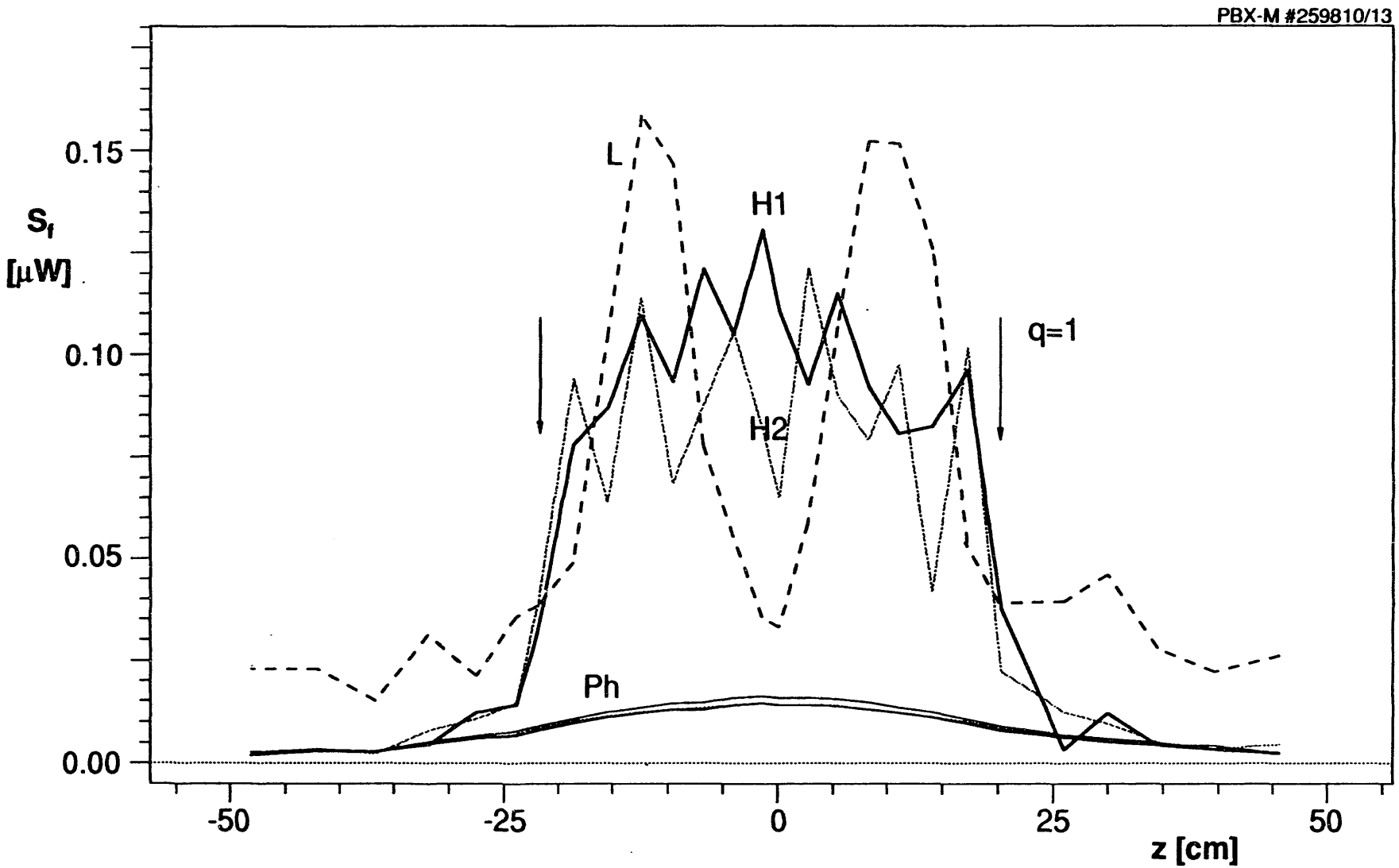

Fig. 13

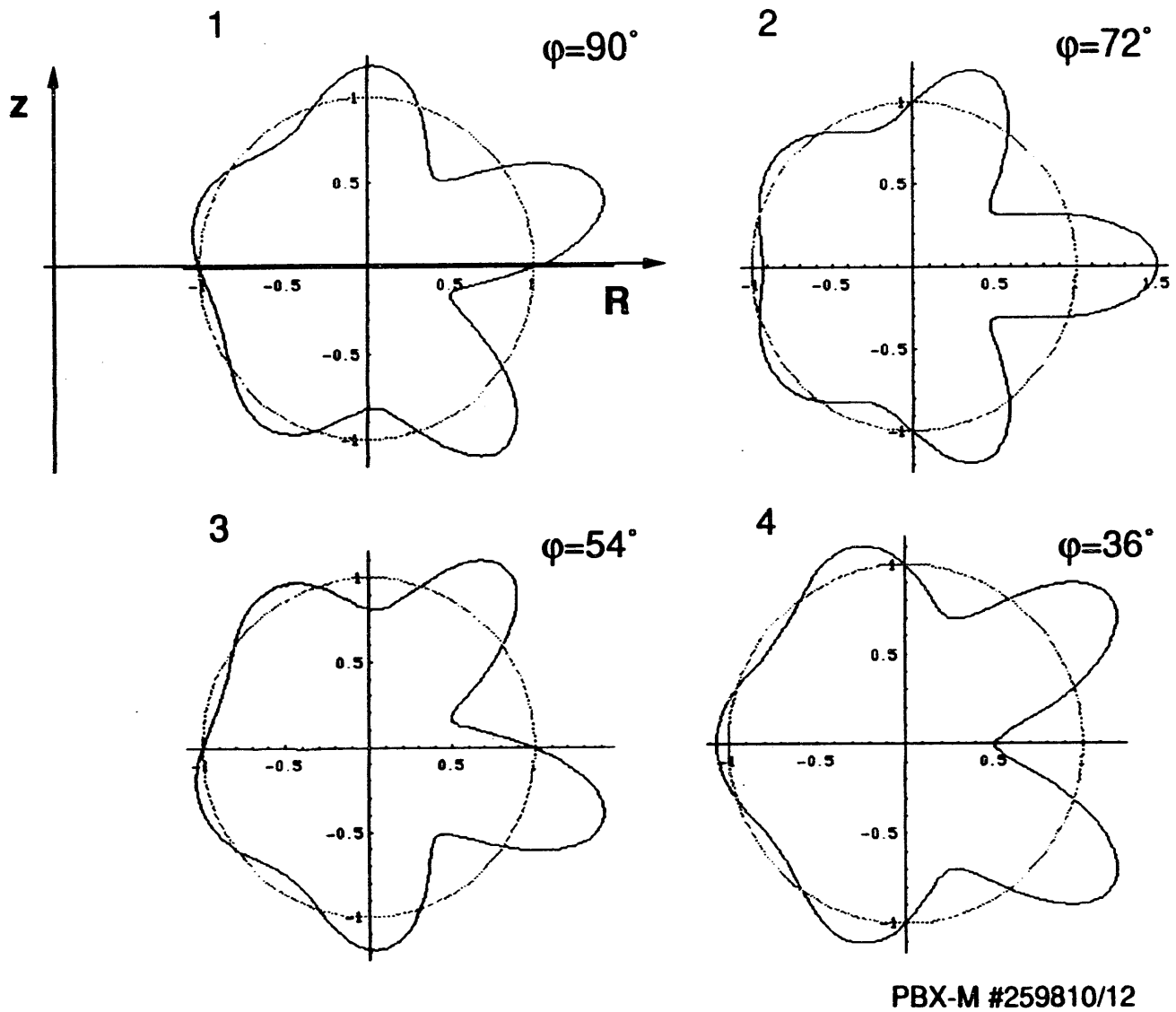

Fig. 14

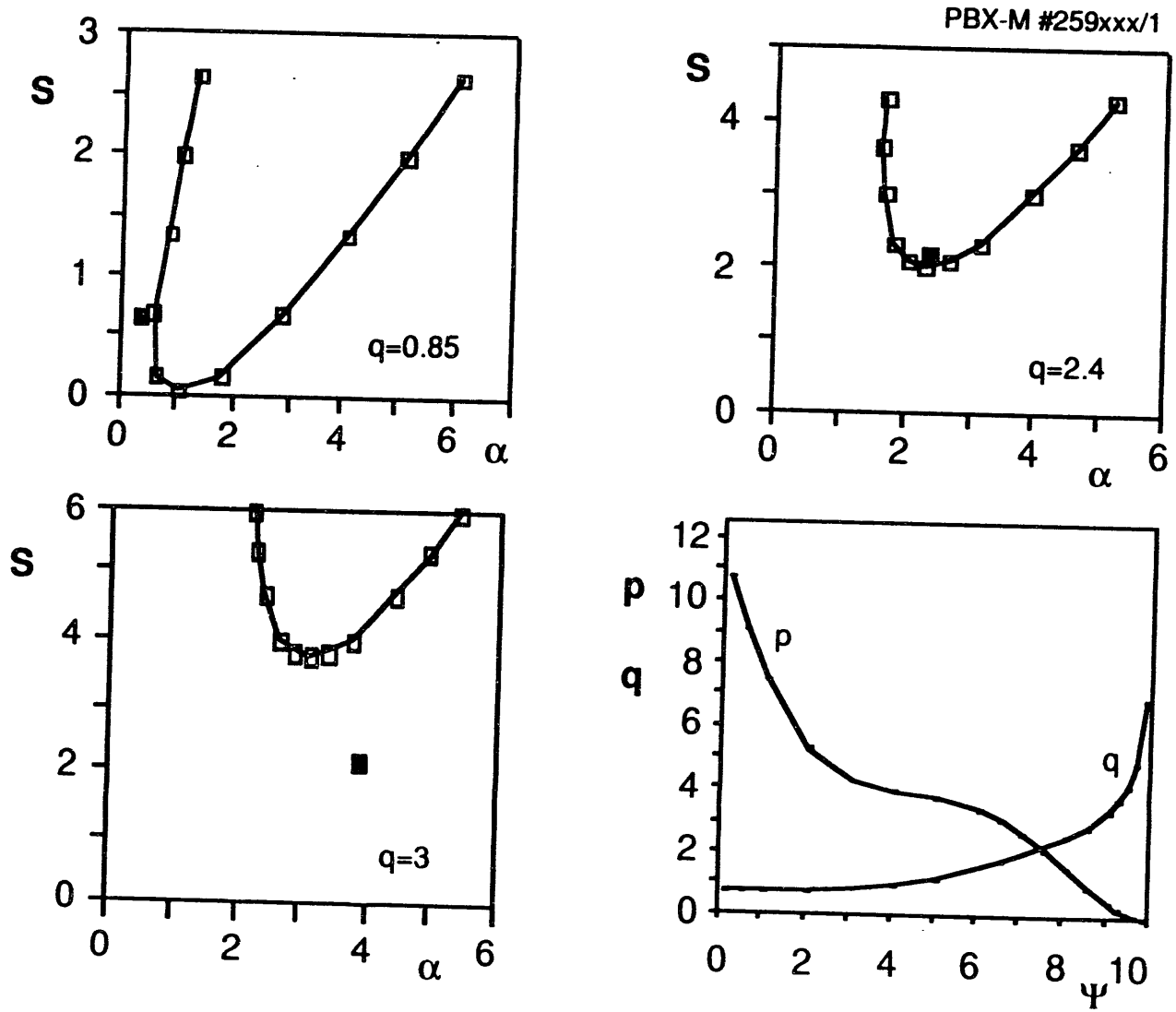

Fig. 15

EXTERNAL DISTRIBUTION IN ADDITION TO UC-420

Dr. F. Paoloni, Univ. of Wollongong, AUSTRALIA
Prof. M.H. Brennan, Univ. of Sydney, AUSTRALIA
Plasma Research Lab., Australian Nat. Univ., AUSTRALIA
Prof. I.R. Jones, Flinders Univ, AUSTRALIA
Prof. F. Cap, Inst. for Theoretical Physics, AUSTRIA
Prof. M. Heindler, Institut für Theoretische Physik, AUSTRIA
Prof. M. Goossens, Astronomisch Instituut, BELGIUM
Ecole Royale Militaire, Lab. de Phy. Plasmas, BELGIUM
Commission-European, DG. XII-Fusion Prog., BELGIUM
Prof. R. Boucique, Rijksuniversiteit Gent, BELGIUM
Dr. P.H. Sakanaka, Instituto Fisica, BRAZIL
Instituto Nacional De Pesquisas Espaciais-INPE, BRAZIL
Documents Office, Atomic Energy of Canada Ltd., CANADA
Dr. M.P. Bachynski, MPB Technologies, Inc., CANADA
Dr. H.M. Skarsgard, Univ. of Saskatchewan, CANADA
Prof. J. Teichmann, Univ. of Montreal, CANADA
Prof. S.R. Sreenivasan, Univ. of Calgary, CANADA
Prof. T.W. Johnston, INRS-Energie, CANADA
Dr. R. Bolton, Centre canadien de fusion magnétique, CANADA
Dr. C.R. James,, Univ. of Alberta, CANADA
Dr. P. Lukác, Komenského Universzita, CZECHO-SLOVAKIA
The Librarian, Culham Laboratory, ENGLAND
Library, R61, Rutherford Appleton Laboratory, ENGLAND
Mrs. S.A. Hutchinson, JET Library, ENGLAND
Dr. S.C. Sharma, Univ. of South Pacific, FIJI ISLANDS
P. Mähönen, Univ. of Helsinki, FINLAND
Prof. M.N. Bussac, Ecole Polytechnique,, FRANCE
C. Mouttet, Lab. de Physique des Milieux Ionisés, FRANCE
J. Radet, CEN/CADARACHE - Bat 506, FRANCE
Prof. E. Economou, Univ. of Crete, GREECE
Ms. C. Rinni, Univ. of Ioannina, GREECE
Dr. T. Mual, Academy Bibliographic Ser., HONG KONG
Preprint Library, Hungarian Academy of Sci., HUNGARY
Dr. B. DasGupta, Saha Inst. of Nuclear Physics, INDIA
Dr. P. Kaw, Inst. for Plasma Research, INDIA
Dr. P. Rosenau, Israel Inst. of Technology, ISRAEL
Librarian, International Center for Theo Physics, ITALY
Miss C. De Palo, Associazione EURATOM-ENEA , ITALY
Dr. G. Grosso, Istituto di Fisica del Plasma, ITALY
Prof. G. Rostangni, Istituto Gas Ionizzati Del Cnr, ITALY
Dr. H. Yamato, Toshiba Res & Devel Center, JAPAN
Prof. I. Kawakami, Hiroshima Univ., JAPAN
Prof. K. Nishikawa, Hiroshima Univ., JAPAN
Director, Japan Atomic Energy Research Inst., JAPAN
Prof. S. Itoh, Kyushu Univ., JAPAN
Research Info. Ctr., National Instit. for Fusion Science, JAPAN
Prof. S. Tanaka, Kyoto Univ., JAPAN
Library, Kyoto Univ., JAPAN
Prof. N. Inoue, Univ. of Tokyo, JAPAN
Secretary, Plasma Section, Electrotechnical Lab., JAPAN
S. Mori, Technical Advisor, JAERI, JAPAN
Dr. O. Mitarai, Kumamoto Inst. of Technology, JAPAN
J. Hyeon-Sook, Korea Atomic Energy Research Inst., KOREA
D.I. Choi, The Korea Adv. Inst. of Sci. & Tech., KOREA
Prof. B.S. Liley, Univ. of Waikato, NEW ZEALAND
Inst of Physics, Chinese Acad Sci PEOPLE'S REP. OF CHINA
Library, Inst. of Plasma Physics, PEOPLE'S REP. OF CHINA
Tsinghua Univ. Library, PEOPLE'S REPUBLIC OF CHINA
Z. Li, S.W. Inst Physics, PEOPLE'S REPUBLIC OF CHINA
Prof. J.A.C. Cabral, Instituto Superior Tecnico, PORTUGAL
Dr. O. Petrus, AL I CUZA Univ., ROMANIA
Dr. J. de Villiers, Fusion Studies, AEC, S. AFRICA
Prof. M.A. Hellberg, Univ. of Natal, S. AFRICA
Prof. D.E. Kim, Pohang Inst. of Sci. & Tech., SO. KOREA
Prof. C.I.E.M.A.T, Fusion Division Library, SPAIN
Dr. L. Stenflo, Univ. of UMEA, SWEDEN
Library, Royal Inst. of Technology, SWEDEN
Prof. H. Wilhelmson, Chalmers Univ. of Tech., SWEDEN
Centre Phys. Des Plasmas, Ecole Polytech, SWITZERLAND
Bibliotheek, Inst. Voor Plasma-Fysica, THE NETHERLANDS
Asst. Prof. Dr. S. Cakir, Middle East Tech. Univ., TURKEY
Dr. V.A. Glukhikh,Sci. Res. Inst. Electrophys.I Apparatus, USSR
Dr. D.D. Ryutov, Siberian Branch of Academy of Sci., USSR
Dr. G.A. Eliseev, I.V. Kurchatov Inst., USSR
Librarian, The Ukr.SSR Academy of Sciences, USSR
Dr. L.M. Kovrizhnykh, Inst. of General Physics, USSR
Kernforschungsanlage GmbH, Zentralbibliothek, W. GERMANY
Bibliothek, Inst. Für Plasmaforschung, W. GERMANY
Prof. K. Schindler, Ruhr-Universität Bochum, W. GERMANY
Dr. F. Wagner, (ASDEX), Max-Planck-Institut, W. GERMANY
Librarian, Max-Planck-Institut, W. GERMANY
Prof. R.K. Janev, Inst. of Physics, YUGOSLAVIA

END

DATE FILMED

9/20/93